




Spectroscopic survey of higher-lying states of B_c meson family

Xue-Jian Li^{1,2,3,5,a}, Yu-Shuai Li^{1,2,3,5,b}, Fu-Lai Wang^{1,2,3,5,c}, Xiang Liu^{1,2,3,4,5,d} 

¹ School of Physical Science and Technology, Lanzhou University, Lanzhou 730000, China

² Lanzhou Center for Theoretical Physics, Key Laboratory of Theoretical Physics of Gansu Province, Lanzhou University, Lanzhou 730000, China

³ Key Laboratory of Quantum Theory and Applications of MoE, Lanzhou University, Lanzhou 730000, China

⁴ MoE Frontiers Science Center for Rare Isotopes, Lanzhou University, Lanzhou 730000, China

⁵ Research Center for Hadron and CSR Physics, Lanzhou University and Institute of Modern Physics of CAS, Lanzhou 730000, China

Received: 16 September 2023 / Accepted: 7 November 2023 / Published online: 27 November 2023
© The Author(s) 2023

Abstract In this work, we investigate the complete spectroscopy of the B_c mesons, with a special focus on the consideration of the unquenched effects. To account for such effects, we employ the modified Godfrey–Isgur model and introduce a screening potential. The resulting mass spectrum of the concerned higher B_c states is then presented, showing significant deviations after considering the unquenched effects. This emphasizes the importance of considering the unquenched effects when studying of the higher B_c mesons. Furthermore, we determine the corresponding spatial wave functions of these B_c mesons, which have practical applications in subsequent studies of their decays. These decays include two-body Okuba–Zweig–Iizuka allowed strong decays, dipion transitions between B_c mesons, radiative decays, and some typical weak decays. With the ongoing high-luminosity upgrade of the Large Hadron Collider, we expect the discovery of additional B_c states in the near future. The knowledge gained from the mass spectrum and the different decay modes will undoubtedly provide valuable insights for future experimental explorations of these higher B_c mesons.

1 Introduction

The study of hadron spectroscopy offers a unique avenue to deepen our understanding of the non-perturbative nature of the strong interaction. Over the past few decades, significant progress has been made, both experimentally and theoretically, leading to extensive investigations of the exotic

hadronic states, such as the charmonium-like states XYZ and the hidden-charm pentaquark states P_c/P_{cs} [1–14]. Moreover, notable observations of light flavor hadrons by the BESIII Collaboration [15], as well as heavy flavor hadrons by the LHCb [16–19] and Belle collaborations [20–22], indicate that the construction of the conventional hadron family is an ongoing endeavor. The abundance of these phenomena in hadron spectroscopy underscores the field’s position at the forefront of precision particle physics.

In contrast to the well-established charmonium and bottomonium families, the B_c meson family remains relatively unexplored, with only a few low-lying B_c states reported in experiments. Pivotal theoretical contributions were made by Refs. [23,24], which proposed the experimental detection of the B_c mesons through the hadron colliders. In 1998, the CDF Collaboration reported the observation of a B_c meson with the mass of $M = (6.40 \pm 0.39 \pm 0.13)$ GeV, identified via the $B^\pm \rightarrow J/\psi \ell^\pm \nu$ decay [25]. This measured mass is consistent with expectations for the ground state of the B_c meson [24,26–29]. However, the full establishment of the B_c meson family remains a formidable task, requiring extensive efforts to identify and explore its properties.

The B_c meson family has been the focus of extensive investigations, both experimentally and theoretically, since its initial observation by the CDF Collaboration in 1998 via the $B^\pm \rightarrow J/\psi \ell^\pm \nu$ decay [25]. Prior to that, searches for the B_c mesons were conducted by the LEP [30–32] and CDF [33] collaborations. Subsequent experimental efforts by various collaborations have confirmed the existence of the B_c mesons through different decay channels, such as the $B_c \rightarrow J/\psi \pi$, $B_c^+ \rightarrow J/\psi \pi^+ \pi^- \pi^+$, $B_c^+ \rightarrow B_s^0 \pi^+$, and $B_c \rightarrow J/\psi K^+ K^- \pi^+$ processes [25,34–42].

In 2014, the ATLAS Collaboration reported the observation of a structure consistent with the predicted $B_c(2S)$

^a e-mail: xjli21@lzu.edu.cn

^b e-mail: liysh20@lzu.edu.cn

^c e-mail: wangfl2016@lzu.edu.cn

^d e-mail: xiangliu@lzu.edu.cn (corresponding author)

state, with a mass of (6842 ± 9) MeV [43]. Additionally, the CMS and LHCb collaborations observed the excited $B_c(2^1S_0)$ and $B_c(2^3S_1)$ states in the $B_c^+\pi^+\pi^-$ invariant mass spectrum, with masses determined as (6872.1 ± 2.2) MeV and (6841.2 ± 1.5) MeV, respectively [44, 45]. However, the current Particle Data Group (PDG) includes only two B_c mesons, namely the $B_c(1S)$ and $B_c(2S)$ states [46]. The limited experimental knowledge of the complete B_c family, particularly the higher excited B_c states, highlights the necessity for further studies in this area.

The study of the B_c meson family plays a crucial role in advancing our understanding of the strong interaction and the non-perturbative regime of quantum chromodynamics (QCD). With the forthcoming high-luminosity upgrade of the Large Hadron Collider (LHC), there are promising opportunities to investigate the higher excited states of the B_c meson, and it is anticipated that additional experimental data will become available in the near future.

Some theoretical studies have examined the B_c spectrum using the quenched quark models, as discussed in references [47–53]. Among these models, the Godfrey–Isgur (GI) model [47], proposed by Stephen Godfrey and Nathan Isgur in 1985, has demonstrated notable success in describing the spectra of low-lying hadrons. Additionally, other quenched quark models have exhibited remarkable achievements in predicting the spectra of low-lying mesons. However, it is now widely acknowledged that the unquenched effects play a significant role, as they can resolve the low-mass puzzles of several hadrons, such as the $D_{s0}(2317)$ [54–57], $D_{s1}(2460)$ [55, 58], $X(3872)$ [59–61], and $\Lambda_c(2940)$ [62]. Therefore, when exploring the spectroscopy of higher excited states of the B_c meson, it is imperative to consider the unquenched effects as well.

In this study, we employ the modified Godfrey–Isgur (MGI) model [63–67] to account for the unquenched effects. To reflect such effects, we utilize a screening potential introduced in Refs. [68, 69]. Furthermore, this method has been applied to the study of bottomonia [65] and charmonia family [66, 67], and has yielded the predictions, providing valuable guidance for experimental investigations. It should be noted that the couple channel effect and the screening potential have a similar effect on the hadron masses, i.e. the higher excited state masses are reduced [60, 70, 71]. In the following section, we provide a concise overview of the MGI model and present the mass spectrum of the B_c family, along with a comparison to the quenched quark model, in order to elucidate the distinctions between the two models. Furthermore, we present the numerical spatial wave functions obtained from the MGI model, which serve as crucial inputs for investigating various properties. Specifically, we calculate the magnetic moments of the higher excited B_c states to reveal their internal structures. This analysis can be valuable in differentiating between conventional B_c states and exotic B_c -like

molecular tetraquark states with identical quantum numbers and similar masses.

To provide a comprehensive theoretical analysis, we also calculate the two-body Okubo–Zweig–Iizuka (OZI)-allowed strong decays, dipion decays, radiative decays, and typical weak decays by employing the numerical spatial wave functions of the relevant mesons. In the concrete calculations, the quark pair creation (QPC) model [72–75] is utilized to describe the behavior of the two-body OZI-allowed strong decays, while the electric dipole (E1) and magnetic dipole (M1) radiative transitions are analyzed by considering the radial decays of the higher excited B_c states. For the investigations of dipion transitions, we adopt the quantum chromodynamics multipole expansion (QCDME) method. Additionally, we employ the covariant light-front quark model (CLFQM) to calculate a series of weak transition form factors and their corresponding weak decays. The spatial wave functions play a crucial role in these decay processes, and by utilizing the MGI model, we obtain reliable numerical results. As experimental data continue to accumulate, these decay processes can be further explored and potentially measured with higher precision.

This paper is organized as follows. In Sect. 2, we present our analysis of the mass spectrum of B_c mesons using the MGI model with the screening effects, and provide the associated numerical spatial wave functions. Section 3 is dedicated to the predictions of two-body OZI-allowed strong decays of the considered B_c mesons by employing the QPC model. In Sect. 4, we investigate the dipion transitions between the B_c states. Section 5 focuses on the predictions of the decay widths for the E1 and M1 radiative transitions and the magnetic moments of these higher B_c mesons. Furthermore, in Sect. 6, we explore some concerned weak transition form factors and the corresponding weak decays for the B_c meson. Finally, our findings are summarized in Sect. 7.

2 Mass spectrum and the corresponding spatial wave functions

In this study, we employ the MGI model to calculate the mass spectrum of the higher excited B_c states. To accurately account for the screening effects, we incorporate a screening potential into our calculations. Furthermore, we derive the corresponding numerical spatial wave functions, which play a pivotal role in the investigations of the decay properties of the B_c states.

2.1 The mass spectrum

To obtain the mass spectrum of the B_c mesons, we apply the MGI model by introducing the screening potential [63–67, 76, 77]. The involved Hamiltonian is

$$\tilde{H} = (p^2 + m_1^2)^{1/2} + (p^2 + m_2^2)^{1/2} + V_{\text{eff}}(\mathbf{p}, \mathbf{r}), \quad (2.1)$$

where m_1 and m_2 denote the masses of the b and c quarks, respectively. $V_{\text{eff}}(\mathbf{p}, \mathbf{r}) = H^{\text{conf}} + H^{\text{hyp}} + H^{\text{so}}$ is the effective potential representing the $q'\bar{q}$ interaction.

In the non-relativistic limit, $V_{\text{eff}}(\mathbf{p}, \mathbf{r})$ is transformed into the familiar nonrelativistic potential $V_{\text{eff}}(r)$, which can be written as

$$V_{\text{eff}}(r) = H^{\text{conf}} + H^{\text{hyp}} + H^{\text{so}}, \quad (2.2)$$

where

$$H^{\text{conf}} = c + \frac{b(1 - e^{-\mu r})}{\mu} - \frac{4\alpha_s(r)}{3r} \quad (2.3)$$

is the spin-independent potential, which includes the screening potential and the Coulomb-like potential. Here, $\alpha_s(r)$ is a running coupling constant, and μ is a parameter which stands for the strength of the screening effects. The colour hyperfine interaction is given by

$$H^{\text{hyp}} = \frac{4\alpha_s(r)}{3m_1m_2} \left[\frac{8\pi}{3} \mathbf{S}_1 \cdot \mathbf{S}_2 \delta^3(\mathbf{r}) + \frac{1}{r^3} \left(\frac{3\mathbf{S}_1 \cdot \mathbf{r} \mathbf{S}_2 \cdot \mathbf{r}}{r^2} - \mathbf{S}_1 \cdot \mathbf{S}_2 \right) \right], \quad (2.4)$$

where $\mathbf{S}_{1(2)}$ is the spin of quark or antiquark. And $H^{\text{so}} = H^{\text{so(cm)}} + H^{\text{so(tp)}}$ is the spin-orbit interaction, where

$$H^{\text{so(cm)}} = \frac{4\alpha_s(r)}{3} \frac{1}{r^3} \left(\frac{\mathbf{S}_1}{m_1^2} + \frac{\mathbf{S}_2}{m_2^2} + \frac{\mathbf{S}_1 + \mathbf{S}_2}{m_1m_2} \right) \cdot \mathbf{L} \quad (2.5)$$

is the color-magnetic term resulting from the one-gluon exchange, while

$$H^{\text{so(tp)}} = -\frac{1}{2r} \frac{\partial H^{\text{conf}}}{\partial r} \left(\frac{\mathbf{S}_1}{m_1^2} + \frac{\mathbf{S}_2}{m_2^2} \right) \cdot \mathbf{L} \quad (2.6)$$

denotes the Thomas precession term with the screening effects, where \mathbf{L} is the orbital angular momentum between quark and antiquark. In addition, we need to smear the screened potential $S(r) = \frac{b(1-e^{-\mu r})}{\mu} + c$ and the Coulomb-like potential $G(r) = -\frac{4\alpha_s(r)}{3r}$ by

$$\tilde{S}(r)/\tilde{G}(r) = \int d^3\mathbf{r}' \rho(\mathbf{r} - \mathbf{r}') S(r')/G(r'), \quad (2.7)$$

where

$$\rho(\mathbf{r} - \mathbf{r}') = \frac{\sigma^3}{\pi^{3/2}} \exp\left[-\sigma^2(\mathbf{r} - \mathbf{r}')^2\right] \quad (2.8)$$

is the smearing function, and σ is a smearing parameter. Then, we introduce the momentum dependent factors as follows

$$\begin{aligned} \tilde{G}(r) &\rightarrow \left(1 + \frac{p^2}{E_1 E_2}\right)^{1/2} \tilde{G}(r) \left(1 + \frac{p^2}{E_1 E_2}\right)^{1/2}, \\ \tilde{V}_i(r) &\rightarrow \left(\frac{m_1 m_2}{E_1 E_2}\right)^{1/2+\epsilon_i} \tilde{V}_i(r) \left(\frac{m_1 m_2}{E_1 E_2}\right)^{1/2+\epsilon_i} \end{aligned} \quad (2.9)$$

with $E_{1(2)} = (p^2 + m_{1(2)}^2)^{1/2}$, where ϵ_i correspond to different types of the interactions, and $\tilde{V}_i(r)$ are the effective potentials included in Eqs. (2.4)–(2.6).

For mesons composed of heavy quarks with equal masses, such as the charmonium and bottomonium states, the L - S coupling scheme is appropriate and the meson state can be labeled by the notation $n^{2S+1}L_J$. However, for mesons with constituents of different masses, such as the B_c mesons, the spin-dependent terms in the Hamiltonian can mix the spin-singlet and spin-triplet states, and the resulting mixing states can be expressed as

$$\begin{aligned} L' &= {}^1L_J \cos \theta + {}^3L_J \sin \theta, \\ L &= -{}^1L_J \sin \theta + {}^3L_J \cos \theta, \end{aligned} \quad (2.10)$$

where θ represents the mixing angle.

To solve the Schrödinger equation [78, 79], we use the simple harmonic oscillator (SHO) wave functions as a set of complete bases, i.e.,

$$\begin{aligned} \Psi_{nLM_L}(\mathbf{r}) &= R_{nL}(r, \beta) Y_{L, M_L}(\Omega_{\mathbf{r}}), \\ \Psi_{nLM_L}(\mathbf{p}) &= R_{nL}(p, \beta) Y_{L, M_L}(\Omega_{\mathbf{p}}), \end{aligned} \quad (2.11)$$

where

$$\begin{aligned} R_{nL}(r, \beta) &= \beta^{\frac{3}{2}} \sqrt{\frac{2n!}{\Gamma(n+L+\frac{3}{2})}} (\beta r)^L e^{-\frac{r^2\beta^2}{2}} L_n^{L+\frac{1}{2}}(\beta^2 r^2), \\ R_{nL}(p, \beta) &= \frac{(-1)^n (-i)^L}{\beta^{\frac{3}{2}}} e^{-\frac{p^2}{2\beta^2}} \sqrt{\frac{2n!}{\Gamma(n+L+\frac{3}{2})}} \left(\frac{p}{\beta}\right)^L \\ &\quad \times L_n^{L+\frac{1}{2}}\left(\frac{p^2}{\beta^2}\right). \end{aligned} \quad (2.12)$$

Here, the radial wave functions are denoted by $R_{nL}(r, \beta)$ and $R_{nL}(p, \beta)$ in the coordinate and momentum spaces, respectively. $Y_{L, M_L}(\Omega_{\mathbf{r}})$ and $Y_{L, M_L}(\Omega_{\mathbf{p}})$ stand for the spherical harmonic functions, and $L_n^{L+\frac{1}{2}}(x)$ is the Laguerre polynomial. β is a phenomenological parameter in the SHO wave function, and we set it to be $\beta = 0.5$ GeV in the calculation.

In Table 1, we list the reported experimental data [46] of the masses of bottom-charmed, charmonium, bottomonium, charmed, charmed-strange, bottom, and bottom-strange mesons,

Table 1 The masses (in units of MeV) of the experimental values and our obtained results of the heavy flavor mesons in this work

Mesons	States	Experimental values [46]	This work	
B_c	$1^1 S_0$	6274.47 ± 0.44	6271	
	$2^1 S_0$	6871.2 ± 1	6855	
	$c\bar{c}$	$1^1 S_0$	2983.9 ± 0.4	2969
		$1^3 S_1$	3096.9 ± 0.006	3097
		$1^3 P_0$	3414.71 ± 0.3	3425
		$1^3 P_1$	3510.67 ± 0.05	3497
		$1^1 P_1$	3525.38 ± 0.11	3516
		$1^3 P_2$	3556.17 ± 0.07	3554
	$2^1 S_0$	3637.5 ± 1.1	3616	
$b\bar{b}$	$2^3 S_1$	3686.1 ± 0.06	3668	
	$1^1 S_0$	9398.7 ± 2.0	9415	
	$1^3 S_1$	9460.3 ± 0.26	9466	
	$1^3 P_0$	$9859.4 \pm 0.42 \pm 0.31$	9851	
	$1^3 P_1$	$9892.8 \pm 0.26 \pm 0.31$	9880	
	$1^1 P_1$	9899.3 ± 0.8	9887	
	$1^3 P_2$	$9912.2 \pm 0.26 \pm 0.31$	9903	
	$2^1 S_0$	9999 ± 6.3	9991	
	$2^3 S_1$	10023.26 ± 0.31	10012	
	D	$1^1 S_0$	1864.84 ± 0.05	1862
$1^3 S_1$		2006.85 ± 0.05	2042	
$1^3 P_0$		2343 ± 10	2291	
$1P_1$		2412 ± 9	2387	
$1P'_1$		2422.1 ± 0.6	2467	
$1^3 P_2$		2461.1 ± 0.7	2474	
$2^1 S_0$		2549 ± 19	2541	
$2^3 S_1$		2627 ± 10	2607	
D_s		$1^1 S_0$	1968.35 ± 0.07	1968
		$1^3 S_1$	2112.2 ± 0.4	2129
	$1^3 P_0$	2317.8 ± 0.5	2416	
	$1P_1$	2459.5 ± 0.6	2518	
	$1P'_1$	2535.11 ± 0.06	2545	
	$1^3 P_2$	2569.1 ± 0.8	2588	
	$2^1 S_0$	2591 ± 13	2643	
	$2^3 S_1$	2714 ± 5	2704	
B	$1^1 S_0$	5279.66 ± 0.12	5308	
	$1^3 S_1$	5324.71 ± 0.21	5372	
	$1^3 P_2$	5737.2 ± 0.7	5760	
B_s	$1^1 S_0$	5366.92 ± 0.10	5391	
	$1^3 S_1$	5415.4 ± 1.8	5451	
	$1^3 P_2$	5839.86 ± 0.12	5868	

Table 2 The fitting parameters of the potential model in this work. Besides, the quark masses are chosen as $m_u = m_d = 220$ MeV, $m_s = 419$ MeV, $m_c = 1628$ MeV, and $m_b = 4977$ MeV [52]

Parameters	Values	Parameters	Values
b	0.2053 GeV^2	ϵ_t	0.5034
c	-0.2677 GeV	$\epsilon_{so(V)}$	-0.3105
μ	0.0684 GeV	$\epsilon_{so(S)}$	-0.3195
ϵ_c	-0.1981		

the experimental data in Table 1, we can obtain the mass spectrum of the B_c mesons. Here, the accuracy of the fitting data is judged based on the χ^2 criterion as follows

$$\chi^2 = \sum_i \frac{(m_i^{\text{Th}} - m_i^{\text{Exp}})^2}{m_i^{\text{Er}2}}, \tag{2.13}$$

where m_i^{Th} , m_i^{Exp} , and m_i^{Er} are the theoretical value, the experimental value, and the error of the i th data, respectively. Here, the errors $m_i^{\text{Er}} = 1$ MeV are the uniform values for all considered mesons. In the absence of experimental data on the masses of the B_c mesons, we used the experimental data of other heavy flavor mesons listed in Table 1 to fit the parameters of the model. To make the mesons act in the same proportions in our fit, we chose a universe value of 1 MeV as the uncertainty. Thus, in this work we used it only as a mathematical tool to fit the model parameters, rather than a χ^2 fit in the usual sense. In this case, we have not given the $\chi^2/\text{d.o.f.}$ value and have not considered the uncertainties of the parameters.

In Table 2, we present the fitted parameters of the MGI model, and these parameters were determined by selecting the minimum χ^2 value. By utilizing the parameters in Table 2, we can calculate the mass spectrum of the B_c mesons, which are displayed in Table 3. In addition to the mass spectrum, the Table 3 also includes the mixing angles of the P -wave, D -wave, and F -wave B_c mesons. Furthermore, we provide a comparison with other theoretical studies [48,52,80,81].

In Fig. 1, we present a comparative analysis of the B_c meson mass spectrum, considering both the screening effects and the results obtained by the GI model [52]. Our findings reveal the significant impact of the screening effects on the mass spectrum of the higher excited B_c states, as compared to the predictions based solely on the GI model [52]. Several notable examples are highlighted below:

- (i) The $B_c(4^1 S_0)$ and $B_c(4^3 S_1)$ states exhibit mass reductions of approximately 76 MeV and 76 MeV, respectively, in our calculations compared to the GI model predictions [52].

which are quoted from the PDG [46] and are used to fit the parameters of the MGI model. Due to the limited availability of experimental data for the B_c mesons, we also include experimental data from other mesons as auxiliary. By fitting

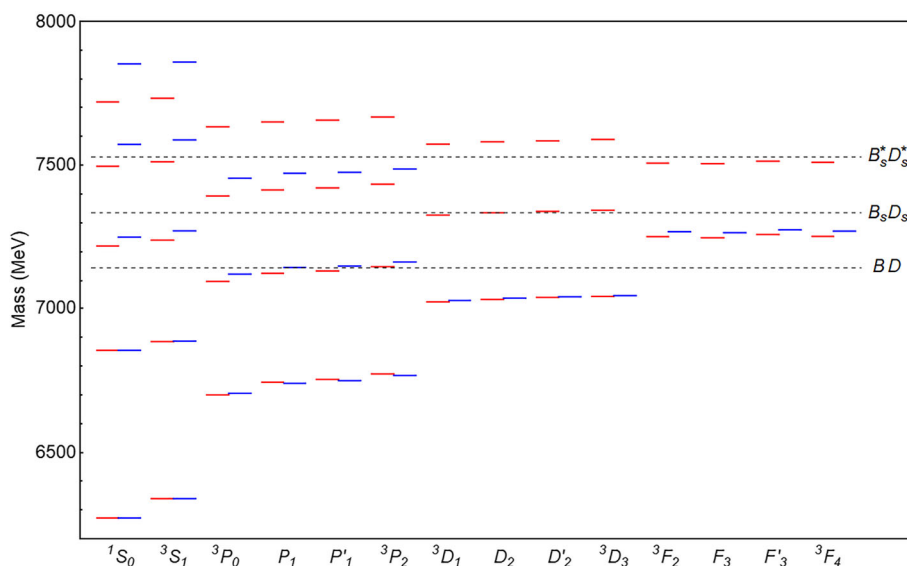
Table 3 The obtained masses of the B_c states and comparison with other results and experimental data. Here, the masses are given in units of MeV

States	Experiments	This work	GI [52]	Ref. [53]	Ref. [80]	Ref. [81]
$1^1 S_0$	6274	6271	6271	6275	6275	6277
$2^1 S_0$	6871	6855	6855	6866	6853	6867
$3^1 S_0$		7220	7250	7253	7222	7228
$4^1 S_0$		7496	7572	7572	7484	
$5^1 S_0$		7722	7854			
$1^3 S_1$		6338	6338	6329	6339	6332
$2^3 S_1$		6886	6887	6897	6920	6911
$3^3 S_1$		7240	7272	7279	7283	7272
$4^3 S_1$		7512	7588	7595	7543	
$5^3 S_1$		7735	7860			
$1^3 P_0$		6701	6706			6705
$1^3 P_2$		6773	6768			6762
$1 P_1$		6745	6741			6739
$1 P'_1$		6754	6750			6748
θ_{1p}		35.2°	22.4°			32.2°
$2^3 P_0$		7097	7122	6692		7112
$2^3 P_2$		7148	7164	6750		7163
$2 P_1$		7125	7145	6730		7144
$2 P'_1$		7133	7150	6738		7149
θ_{2p}		26.5°	18.9°	18.7°		30.9°
$3^3 P_0$		7393	7455	7104		
$3^3 P_2$		7434	7487	7154		
$3 P_1$		7414	7472	7135		
$3 P'_1$		7421	7475	7143		
θ_{3p}		23.6°	18.9°	21.2°		
$4^3 P_0$		7633				
$4^3 P_2$		7667				
$4 P_1$		7650				
$4 P'_1$		7656				
θ_{4p}		22.2°				
$1^3 D_1$		7023	7028			7014
$1^3 D_3$		7042	7045			7035
$1 D_2$		7032	7036			7025
$1 D'_2$		7039	7041			7029
θ_{1D}		-53.4°	45.5°			38.1°
$2^3 D_1$		7327				
$2^3 D_3$		7344				
$2 D_2$		7335				
$2 D'_2$		7340				
θ_{2D}		-48.4°				
$3^3 D_1$		7573				
$3^3 D_3$		7589				
$3 D_2$		7581				
$3 D'_2$		7584				
θ_{3D}		-42.9°				

Table 3 continued

States	Experiments	This work	GI [52]	Ref. [53]	Ref. [80]	Ref. [81]
1^3F_2		7252	7269			
1^3F_4		7253	7271			
$1F_3$		7248	7266			
$1F'_3$		7260	7276			
θ_{1F}		-50.4°	41.4°			
2^3F_2		7507				
2^3F_4		7510				
$2F_3$		7505				
$2F'_3$		7514				
θ_{2F}		-49.5°				

Fig. 1 Mass spectrum of the B_c mesons. Here, the red (left) lines and the blue (right) lines are our obtained results and the results from the GI model [52], respectively, while the short lines denote the thresholds of the $B_{(s)}^{(*)}D_{(s)}^{(*)}$ channels. The masses of the mesons are given in units of MeV



(ii) The impact of the screening effects becomes even more pronounced in the $B_c(5^1S_0)$ and $B_c(5^3S_1)$ states, with a substantial mass difference of up to 120 MeV observed between our results and those obtained without considering the screening effects [52]. This disparity is particularly evident in the higher excited B_c states, as depicted in Fig. 1.

Hence, our findings underscore the necessity of accounting for the unquenched effects when investigating the spectroscopy of higher excited B_c mesons. Future experimental studies with more precise data are expected to provide a valuable opportunity for testing and validating our predictions.

In the preceding subsection, we derived the mass spectrum of the B_c mesons. Furthermore, we can extract the corresponding spatial wave functions, which serve as crucial inputs for investigating their decay properties. Consequently, in this subsection, we present these spatial wave functions to explore their characteristics. The Fig. 2 illustrates the $S/P/D/F$ -wave spatial wave functions of the B_c mesons. Notably, for the spatial wave functions of the S -wave

B_c mesons, noticeable node effects emerge when n exceeds 4, such as $n = 5$, and so on. These node effects can substantially impact certain physical results, which will be discussed in Sect. 3.

3 Two-body OZI-allowed strong decays

In this section, our focus lies on the study of two-body OZI-allowed strong decays of the B_c mesons by employing the QPC model in the concrete calculations. The QPC model, also known as the 3P_0 model, was initially proposed by Micu in 1968 [72] and has since been further developed by the Orsay Group [82–84]. Over time, the QPC model has been extensively utilized to investigate the two-body OZI-allowed strong decays of various hadrons [73–75, 82–84]. Here, we provide a brief introduction to the QPC model, with a specific focus on the transition matrix for the $A \rightarrow B + C$ process.

In the QPC model, the transition matrix for the $A \rightarrow B + C$ decay is defined as follows

$$\langle BC|T|A \rangle = \delta^3(\mathbf{P}_B + \mathbf{P}_C) \mathcal{M}^{M_{JA} M_{JB} M_{JC}}. \tag{3.1}$$

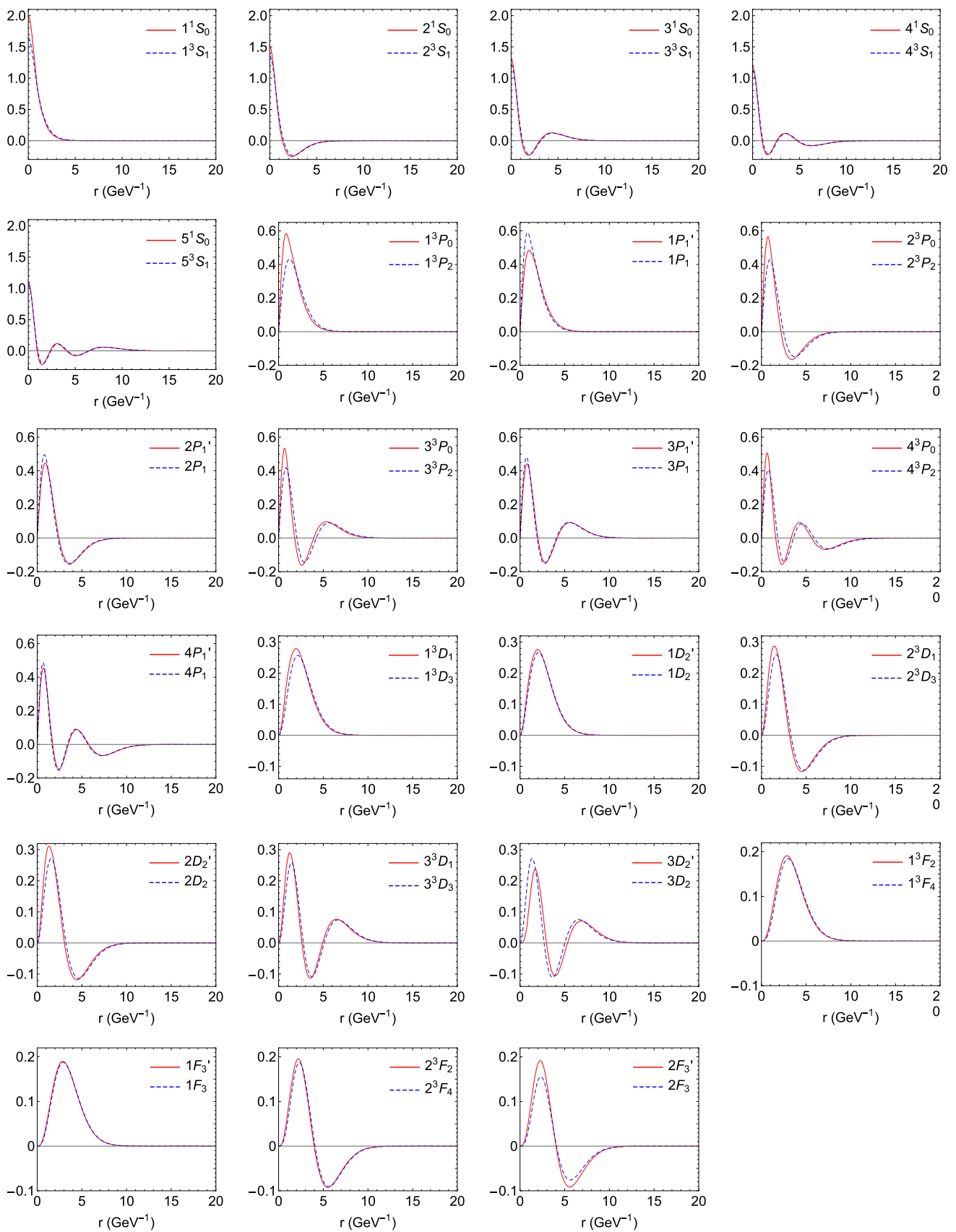


Fig. 2 The obtained spatial wave functions of the concerned B_c mesons. Here, these B_c mesons are classified by the notation $n^{2S+1}L_J$

Here, $\mathcal{M}^{M_{J_A} M_{J_B} M_{J_C}}$ represents the helicity amplitude, while \mathbf{P}_B and \mathbf{P}_C denote the momenta of the daughter mesons B and C , respectively, in the rest frame of the parent meson A . The states $|A\rangle$, $|B\rangle$, and $|C\rangle$ correspond to the mock states associated with mesons A , B , and C , respectively. Furthermore, \mathcal{T} represents the transition operator, which describes the creation of a quark-antiquark pair from the vacuum. In the non-relativistic limit, the transition operator can be expressed as

$$\begin{aligned} \mathcal{T} = & -3\gamma \sum_m \langle 1, m; 1, -m | 0, 0 \rangle \int d\mathbf{p}_3 d\mathbf{p}_4 \delta^3(\mathbf{p}_3 + \mathbf{p}_4) \\ & \times \mathcal{Y}_{lm} \left(\frac{\mathbf{p}_3 - \mathbf{p}_4}{2} \right) \chi_{1,-m}^{34} \phi_0^{34} \left(\omega_0^{34} \right)_{ij} b_{3i}^\dagger(\mathbf{p}_3) d_{4j}^\dagger(\mathbf{p}_4), \end{aligned} \tag{3.2}$$

where the quark and antiquark are represented by indices 3 and 4, respectively. The state $\chi_{1,-m}^{34}$ corresponds to a spin-triplet configuration, while ϕ_0^{34} and ω_0^{34} denote the SU(3) flavor and color singlets, respectively. The parameter γ is a dimensionless constant that characterizes the strength of quark-antiquark pair creation from the vacuum, and its value is determined through the fitting of experimental data. The term $\mathcal{Y}_{lm}(\mathbf{p}) = |\mathbf{p}|^l Y_{lm}(\mathbf{p})$ represents the solid harmonic function. According to the Jacobi–Wick formula [85], the helicity amplitude can be transformed into the partial wave amplitude, which can be expressed as

$$\begin{aligned} \mathcal{M}^{JL}(\mathbf{P}) = & \frac{\sqrt{4\pi(2L+1)}}{2J_A+1} \sum_{M_{J_B} M_{J_C}} \langle L0; JM_{J_A} | J_A M_{J_A} \rangle \\ & \times \langle J_B M_{J_B}; J_C M_{J_C} | J_A M_{J_A} \rangle \mathcal{M}^{M_{J_A} M_{J_B} M_{J_C}}, \end{aligned} \tag{3.3}$$

where L is the orbital angular momentum between final states B and C . The partial width of the $A \rightarrow B + C$ process can be given by

$$\Gamma = \frac{\pi}{4} \frac{|\mathbf{P}_B|}{m_A^2} \sum_{J,L} \left| \mathcal{M}^{JL}(\mathbf{P}) \right|^2, \tag{3.4}$$

where m_A is the mass of the parent meson A .

In addition, the meson wave function is defined as the mock state [86], i.e.,

$$\begin{aligned} & \left| A \left(n^{2S+1} L_{JM_J} \right) \left(\mathbf{p}_A \right) \right\rangle \\ & = \sqrt{2E} \sum_{M_S, M_L} \langle LM_L; SM_S | JM_J \rangle \chi_{SM_S}^A \\ & \times \phi^A \omega^A \int d\mathbf{p}_1 d\mathbf{p}_2 \delta^3(\mathbf{p}_A - \mathbf{p}_1 - \mathbf{p}_2) \\ & \times \Psi_{nLM_L}^A(\mathbf{p}_1, \mathbf{p}_2) |q_1(\mathbf{p}_1) \bar{q}_2(\mathbf{p}_2)\rangle, \end{aligned} \tag{3.5}$$

where $\chi_{SM_S}^A$, ϕ^A , ω^A , and $\Psi_{nLM_L}^A(\mathbf{p}_1, \mathbf{p}_2)$ denote the spin, flavor, color, and spatial wave functions of meson A , respectively. In our concrete calculations, we utilize the numerical spatial wave functions obtained in Sect. 2 as inputs for these mesons. This approach helps to avoid the dependence on the β values by taking a SHO wave function. Furthermore, since experimental width data is lacking, we adopt the value of γ for $q\bar{q}$ as $0.4\sqrt{96\pi}$ from Ref. [87], while the creation strength for $s\bar{s}$ satisfies $\gamma_s = \gamma/\sqrt{3}$.

In Table 4, we present the two-body OZI-allowed strong decay widths and the corresponding branching ratios of the S -wave and P -wave B_c states with $n = 3, 4, 5$ and $n = 3, 4$, respectively. These discussed $B_c(n^1S_0)$ states with $n = 3, 4, 5$ can decay into the B^*D channel. As we increase the principal quantum number n , such as $n = 5$, we observe a significant reduction in the partial width of their decays into the B^*D channel. This reduction is primarily due to the node effects of the corresponding spatial wave functions, as illustrated in Fig. 2. For the $B_c(3^1S_0)$ state, the B^*D is the unique two-body OZI-allowed decay channel around 62 MeV. Thus, the B^*D channel should be the promising channel to observe the $B_c(3^1S_0)$ state. For the $B_c(4^1S_0)$ state, it mainly decays into the BD^* , B^*D , and B^*D^* channels, and whose corresponding branching ratios are more than 99%. For the $B_c(5^1S_0)$ state, it dominantly decays into the BD^* , B^*D , B^*D^* , and $BD(^3P_0)$ channels.

The node effects are more pronounced for the $B_c(n^3S_1)$ mesons compared to the $B_c(n^1S_0)$ mesons, with a notable example being the $B_c(4^3S_1)$ state. Furthermore, for the $B_c(5^3S_1)$ state, the decay widths of the $B_s^*D_s^*$ and $B^*D(1^3P_0)$ channels are 1.7×10^{-3} MeV and 2.5×10^{-3} MeV, respectively, reaching a order of magnitude of 10^{-3} MeV. Thus, it is evident that the node effects in the $B_c(5^3S_1)$ state are more significant than that in the $B_c(5^1S_0)$ state. In the following, we summarize several main points: (i) The total width of the $B_c(3^3S_1)$ state is about 82 MeV, and the main decay channels of the $B_c(3^3S_1)$ state are BD and B^*D ; (ii) The $B_c(4^3S_1)$ state mainly decays into the B^*D , BD^* , and B^*D^* channels, and the BD also has the sizable contribution to the total width; (iii) The main decay modes of the $B_c(5^3S_1)$ state include the B^*D , BD^* , B^*D^* , $BD(1P_1)$, and $BD(1P_1')$ channels, while the dominant decay channel is the B^*D^* with branching ratio 70.1%.

For these $3P$ states of the B_c meson, the partial widths of the $B_s D_s$ and $B_s^* D_s$ decay channels are significantly suppressed. Specifically, for the $B_c(3^3P_0)$ state, the $B_s^* D_s$ channel is kinematically forbidden. Similarly, for the $4P$ states of the B_c meson, the decay channel of $B_s^* D_s^*$ is also kinematically forbidden. Furthermore, for the $B_c(3^3P_2)$ and $B_c(4P_1')$ states, the decay widths of the B^*D and $B(1P_1)D$ channels are 2.6×10^{-3} MeV and 2.3×10^{-3} MeV, respectively, reaching the order of magnitude of 10^{-3} MeV. Our results show that the largest decay width of these discussed

Table 4 Partial widths and the corresponding branching ratios for these two-body OZI-allowed strong decays of the *S*-wave and *P*-wave B_c mesons. Here, the decay widths of the discussed mesons are given in units of MeV

States	Channels	Widths	$\mathcal{B}(\%)$	States	Channels	Widths	$\mathcal{B}(\%)$
3^1S_0	B^*D	62.2	100.0	$3P'_1$	B^*D	34.7	24.6
	Total width	62.2			BD^*	36.5	25.9
4^1S_0	B^*D	26.9	30.2	3^3P_2	B^*D^*	69.1	49.0
	BD^*	31.4	35.2		$B_s^*D_s$	0.8	0.6
	B^*D^*	30.2	33.8		Total width	141.1	
	$B_s^*D_s$	0.01	0.01		BD	2.1	2.1
	$B_sD_s^*$	0.7	0.8		B^*D	2.6×10^{-3}	2.7×10^{-3}
	Total width	89.2			BD^*	14.5	15.0
5^1S_0	B^*D	8.1	11.0	4^3P_0	B^*D^*	79.2	81.6
	BD^*	19.4	26.4		B_sD_s	0.6	0.7
	B^*D^*	42.9	58.5		$B_s^*D_s$	0.6	0.6
	$B_s^*D_s$	0.8	1.1		Total width	97.1	
	$B_sD_s^*$	0.05	0.07		BD	13.2	15.7
	$B_s^*D_s^*$	0.08	0.1		B^*D^*	67.7	80.7
	$B(^3P_0)D$	0.9	1.2		B_sD_s	2.6	3.1
	$B(^3P_2)D$	0.5	0.6		$B_s^*D_s^*$	0.4	0.4
	$BD(^3P_0)$	0.7	0.9		Total width	83.9	
	Total width	73.4			$4P_1$	B^*D	4.5
3^3S_1	BD	25.0	30.4	BD^*		29.7	37.3
	B^*D	57.2	69.6	B^*D^*		34.3	43.1
	Total width	82.2		$B_s^*D_s$		1.1	1.4
4^3S_1	BD	1.8	2.0	$B_sD_s^*$		0.1	0.2
	B^*D	11.6	12.7	$B_s^*D_s^*$	0.04	0.05	
	BD^*	21.9	23.9	$B(1^3P_0)D$	0.05	0.06	
	B^*D^*	54.9	60.1	$B(1P_1)D$	0.06	0.07	
	B_sD_s	0.4	0.4	$B(1^3P_2)D$	9.6	12.1	
	$B_s^*D_s$	0.1	0.2	$BD(1^3P_0)$	0.08	0.1	
	$B_sD_s^*$	0.6	0.6	Total width	79.6		
	Total width	91.4		$4P'_1$	B^*D	7.1	9.6
5^3S_1	BD	0.07	0.1		BD^*	7.0	9.5
	B^*D	2.4	3.6		B^*D^*	39.4	53.2
	BD^*	10.1	15.1		$B_s^*D_s$	1.5	2.0
	B^*D^*	47.0	70.1		$B_sD_s^*$	0.18	0.24
	B_sD_s	0.3	0.4		$B_s^*D_s^*$	0.02	0.03
	$B_s^*D_s$	0.6	0.8		$B(1^3P_0)D$	0.2	0.28
	$B_sD_s^*$	0.09	0.14		$B(1P_1)D$	2.3×10^{-3}	3.1×10^{-3}
	$B_s^*D_s^*$	1.7×10^{-3}	2.5×10^{-3}		$B(1^3P_2)D$	17.8	24.2
	$B(1P_1)D$	0.2	0.3		$BD(1^3P_0)$	0.7	0.9
	$B(1P'_1)D$	0.7	1.0	Total width	73.9		
$B(1^3P_2)D$	0.1	0.2	4^3P_2	BD	3.4	5.4	
$BD(1P_1)$	1.9	2.9		B^*D	1.4	2.2	
$BD(1P'_1)$	3.5	5.2		BD^*	1.3	2.0	

Table 4 continued

States	Channels	Widths	B(%)	States	Channels	Widths	B(%)
3^3P_0	$B^*D(1^3P_0)$	2.5×10^{-3}	3.8×10^{-3}	$3P_1$	B^*D^*	46.1	72.3
	Total width	67.0			B_sD_s	0.1	0.2
	BD	52.5	36.9		$B_s^*D_s$	0.4	0.6
	B^*D^*	89.7	63.1		$B_sD_s^*$	0.2	0.26
	B_sD_s	0.03	0.02		$B_s^*D_s^*$	0.02	0.03
$3P_1$	Total width	142.2		$B(1P_1)D$	4.4	6.9	
	B^*D	18.2	12.3	$B(1P_1')D$	1.1	1.7	
	BD^*	47.5	32.2	$B(1^3P_2)D$	5.4	8.4	
	B^*D^*	81.2	54.9	Total width	63.7		
	$B_s^*D_s$	0.8	0.5				
	Total width	147.7					

$3P$ -wave B_c mesons is the B^*D^* channel, which has the estimated branching ratios of 63.1%, 54.9%, 49.0%, and 81.6% for the $B_c(3^3P_0)$, $B_c(3P_1)$, $B_c(3P_1')$, and $B_c(3^3P_2)$ states, respectively. Thus, we suggest the future experiments to search for the $3P$ -wave B_c mesons by the B^*D^* channel. For the $4P$ states of the B_c meson, the largest decay width is also the B^*D^* channel. Compared with the $3P$ states of the B_c meson, we find the total widths of the $4P$ states are more smaller than these $3P$ states of the B_c meson.

In Table 5, we show the two-body OZI-allowed strong decay widths and the corresponding branching ratios for the D -wave and F -wave B_c states. For these $2D$ states of the B_c meson, no decay channels are significantly suppressed, and the largest decay channels are also different. For $B_c(2^3D_1)$ and $B_c(2D_2')$ states, the largest decay width is also the BD^* channel, whose branching ratios are 59.8% and 69.5%, respectively. However, the largest decay widths of the $B_c(2D_2)$ and $B_c(2^3D_3)$ states are B^*D and B^*D^* channels, respectively. For the $B_c(3D)$ states, the largest decay width is the B^*D^* channel, whose branching ratios are 58.4%, 37.2%, 82.1%, and 64.4% for the $B_c(3^3D_1)$, $B_c(3D_2)$, $B_c(3D_2')$, and $B_c(3^3D_3)$ states, respectively. For the $3D$ states of the B_c meson, the decay widths of some channels are significantly suppressed. Such as the $B_sD_s^*$ channel for the $B_c(3^3D_1)$ state and the B_sD_s channel for the $B_c(3^3D_3)$ state, whose decay widths are 4.7×10^{-3} MeV and 2.3×10^{-4} MeV, respectively.

For the $B_c(1^3F_2)$ and $B_c(1^3F_4)$ states, they can decay into the BD and B^*D channels, and their dominant decay mode is the BD channel. In addition, it is worth noting that the $B_c(1F_3')$ and $B_c(1F_3)$ states can decay into the B^*D channel with the branching ratios 100%, but their decay widths exist obvious difference, which is similar to the decay behaviour of the $B_c(1^3F_2)$ and $B_c(1^3F_4)$ states. The B^*D^* is the dominant decay channel for the $2F$ states of the B_c meson, and the

branching ratios are 71.2%, 48.0%, 58.6%, and 51.4% for the $B_c(2^3F_2)$, $B_c(2F_3)$, $B_c(2F_3')$, and $B_c(2^3F_4)$ states, respectively. The $B_sD_s^*$ is a significantly suppressing channel for the $2F$ states of the B_c meson, especially for the $B_c(2F_3)$ and $B_c(2^3F_4)$ states, whose branching ratios are 2.9×10^{-5} and 2.0×10^{-5} , respectively.

In general, the information on the concerned two-body OZI-allowed strong decays presented of B_c mesons in Tables 4 and 5 can provide valuable guidance for further experimental searches for them.

4 Dipion transitions between B_c mesons

In this section, we investigate the dipion transitions using the QCME approach. The QCME has been widely used to study the dipion or η hadronic transitions between the low-lying heavy quarkonium [65, 88–94]. The idea of this approach is that the QZI-suppressed hadronic transition is represented by the parent heavy quarkonium first emitting a gluon to form an intermediate hybrid state, and then recombining itself to the daughter heavy quarkonium and the light meson(s) (like a η or a pair of pions) with emitting another gluon via the hadronization process.

Following Ref. [90], one can calculate the decay width of the dipion transition as depicted by the following expression:

$$\begin{aligned} \Gamma(A \rightarrow B + \pi^+ \pi^-) &= \delta_{i_1 l_f} \delta_{J_i J_f} (G|c_1|^2 - \frac{2}{3}H|c_2|^2) \\ &\times \left| \sum_l (2l+1) f_{if}^l \begin{pmatrix} l_i & 1 & l \\ 0 & 0 & 0 \end{pmatrix} \begin{pmatrix} l & 1 & l_i \\ 0 & 0 & 0 \end{pmatrix} \right|^2 \\ &+ (2l_i+1)(2l_f+1)(2J_f+1) \end{aligned}$$

Table 5 Partial widths and the corresponding branching ratios for these two-body OZI-allowed strong decays of the D -wave and F -wave B_c states. Here, the decay width of the meson is given in units of MeV

States	Channels	Widths	$\mathcal{B}(\%)$	States	Channels	Widths	$\mathcal{B}(\%)$
2^3D_1	BD	4.9	10.5	1^3F_2	BD	46.8	79.0
	B^*D	14.0	29.7		B^*D	12.5	21.0
	BD^*	28.2	59.8		Total width	59.2	
	Total width	47.2			$1F_3$	B^*D	0.2
$2D_2$	B^*D	24.9	78.1	Total width		0.2	
	BD^*	3.3	10.3	$1F'_3$	B^*D	35.2	100.0
	B^*D^*	3.7	11.6		Total width	35.2	
$2D'_2$	Total width	31.8		1^3F_4	BD	0.7	85.6
	B^*D	34.8	26.3		B^*D	0.1	14.4
	BD^*	91.7	69.5	Total width	0.8		
	B^*D^*	5.5	4.1	2^3F_2	BD	16.6	20.4
Total width	132.0		B^*D		4.0	4.9	
2^3D_3	BD	19.7	23.4		BD^*	1.4	1.7
	B^*D	21.1	25.1		B^*D^*	58.1	71.2
	BD^*	2.7	3.2		B_sD_s	0.5	0.6
	B^*D^*	40.6	48.3		$B_s^*D_s$	0.8	1.0
	Total width	84.2		$B_sD_s^*$	0.1	0.2	
3^3D_1	BD	0.07	0.24	Total width	81.5		
	B^*D	1.1	3.5	$2F_3$	B^*D	13.8	16.3
	BD^*	9.0	29.5		BD^*	28.7	33.7
	B^*D^*	17.8	58.4		B^*D^*	40.9	48.0
	B_sD_s	1.4	4.5	$B_s^*D_s$	1.7	2.0	
	$B_s^*D_s$	0.7	2.2	$B_sD_s^*$	0.2	2.9×10^{-3}	
	$B_sD_s^*$	4.7×10^{-3}	0.01	Total width	85.2		
	$B_s^*D_s^*$	0.5	1.6	$2F'_3$	B^*D	27.1	37.6
	Total width	30.5			BD^*	1.7	2.4
$3D_2$	B^*D	15.0	27.7		B^*D^*	42.2	58.6
	BD^*	18.1	33.4	$B_s^*D_s$	0.5	0.7	
	B^*D^*	20.1	37.2	$B_sD_s^*$	0.5	0.7	
	$B_s^*D_s$	0.4	0.7	Total width	72.0		
	$B_sD_s^*$	0.08	0.16	2^3F_4	BD	8.2	10.2
	$B_s^*D_s^*$	0.5	0.9		B^*D	14.2	17.8
	Total width	54.17			BD^*	15.7	19.7
$3D'_2$	B^*D	0.6	2.3		B^*D^*	40.9	51.4
	BD^*	1.2	4.5	B_sD_s	0.4	0.5	
	B^*D^*	21.0	82.1	$B_s^*D_s$	0.2	0.3	
	$B_s^*D_s$	1.8	7.0	$B_sD_s^*$	1.6×10^{-3}	2.0×10^{-3}	
	$B_sD_s^*$	0.5	2.1	Total width	79.7		
	$B_s^*D_s^*$	0.5	1.9				
	Total width	25.6					
3^3D_3	BD	10.3	16.1				
	B^*D	10.2	15.9				
	BD^*	1.4	2.2				

Table 5 continued

States	Channels	Widths	B(%)	States	Channels	Widths	B(%)
	B^*D^*	41.2	64.4				
	$B_s D_s$	2.3×10^{-4}	3.6×10^{-4}				
	$B_s^* D_s$	0.1	0.2				
	$B_s D_s^*$	0.3	0.5				
	$B_s^* D_s^*$	0.5	0.8				
	Total width	64.0					

$$\begin{aligned} & \times \sum_k (2k + 1) [1 + (-1)^k] \left\{ \begin{matrix} s & l_f & J_f \\ k & J_i & l_i \end{matrix} \right\}^2 H |c_2|^2 \\ & \times \left| \sum_l (2l + 1) f_{if}^l \begin{pmatrix} l_f & 1 & l \\ 0 & 0 & 0 \end{pmatrix} \begin{pmatrix} l & 1 & l_i \\ 0 & 0 & 0 \end{pmatrix} \left\{ \begin{matrix} l_i & l & 1 \\ 1 & k & l_f \end{matrix} \right\} \right|^2, \end{aligned} \tag{4.1}$$

where c_1 and c_2 are undetermined parameters, while $l_{i(f)}$ and $J_{i(f)}$ are the orbital and total angular momenta of meson $A(B)$, respectively. Both mesons A and B possess an identical spin value denoted as s . Furthermore, the phase-space factors, denoted as G and H in this context, are defined as follows:

$$\begin{aligned} G &= \frac{3}{4} \frac{m_f}{m_i} \pi^3 \int dm_{\pi^+\pi^-}^2 K \left(1 - \frac{4m_\pi^2}{m_{\pi^+\pi^-}^2} \right)^{1/2} \\ & \times (m_{\pi^+\pi^-}^2 - 2m_\pi^2)^2, \end{aligned} \tag{4.2}$$

$$\begin{aligned} H &= \frac{1}{20} \frac{m_f}{m_i} \pi^3 \int dm_{\pi^+\pi^-}^2 K \left(1 - \frac{4m_\pi^2}{m_{\pi^+\pi^-}^2} \right)^{1/2} \\ & \times \left[(m_{\pi^+\pi^-}^2 - 4m_\pi^2)^2 \left(1 + \frac{2}{3} \frac{K^2}{m_{\pi^+\pi^-}^2} \right) + \frac{8K^4}{15m_{\pi^+\pi^-}^4} \right. \\ & \left. \times (m_{\pi^+\pi^-}^4 + 2m_\pi^2 m_{\pi^+\pi^-}^2 + 6m_\pi^4) \right], \end{aligned} \tag{4.3}$$

respectively, with

$$K = \frac{\sqrt{((m_i + m_f)^2 - m_{\pi^+\pi^-}^2)((m_i - m_f)^2 - m_{\pi^+\pi^-}^2)}}{2m_i}. \tag{4.4}$$

Here, m_i and m_f are the masses of the initial and final B_c mesons, respectively, while m_π is the mass of the pion. Additionally, the dynamical-associated part f_{if}^l is written as

$$\begin{aligned} f_{if}^l &= \sum_k \frac{1}{m_i - m_{kl}} \int dr r^3 \mathcal{R}_f(r) \mathcal{R}_{kl}(r) \\ & \times \int dr' r'^3 \mathcal{R}_{kl}(r') \mathcal{R}_i(r'), \end{aligned} \tag{4.5}$$

where $\mathcal{R}_i(r)$ and $\mathcal{R}_f(r)$ are the radial wave functions of the parent and daughter B_c mesons, respectively, while $\mathcal{R}_{kl}(r)$ denotes the intermediate vibrational state. m_{kl} is the mass

of the intermediate vibrational state with the radial quantum number k and the orbital angular momentum l .

The spatial wave functions associated with the relevant B_c mesons can be given by utilizing the MGI model as mentioned above. However, for the intermediate vibrational states, the appropriate approach involves resorting to the quark confining string (QCS) model, as established by Refs. [95–97]. The potential of a hybrid state adopted in our calculations is [65]

$$V_{\text{hyb}}(r) = V_G(r) + V_S(r) + [V_n(r) - \sigma(r)r], \tag{4.6}$$

where $V_G(r) = -4\alpha_s(r)/(3r)$ is the one-gluon exchange potential and $V_S(r) = \sigma(r)r + c$ is the color confining potential with

$$\begin{aligned} \alpha_s(r) &= \sum_{k=1}^3 \alpha_k \frac{2}{\sqrt{\pi}} \int_0^{\gamma_k r} e^{-x^2} dx, \\ \sigma(r) &= \frac{b(1 - e^{-\mu r})}{\mu r}. \end{aligned} \tag{4.7}$$

Here, we adopt $\{\alpha_1, \alpha_2, \alpha_3\} = \{0.25, 0.15, 0.20\}$ and $\{\gamma_1, \gamma_2, \gamma_3\} = \{1/2, \sqrt{10}/2, \sqrt{1000}/2\}$ [47,98].

The effective vibrational potential $V_n(r)$ is chosen as [94, 95]

$$V_n(r) = \sigma(r)r \left(1 + \frac{2n\pi}{\sigma(r)[(r - 2d)^2 + 4d^2]} \right)^{1/2} \tag{4.8}$$

with $d = \sigma(r)r^2\alpha_n/(4[m_b + m_c + \sigma(r)r\alpha_n])$. In the calculations, we only consider the lowest string excitation, i.e., $n = 1$. And then, we choose $\alpha_1 = \sqrt{1.5}$ [65].

Before performing the concrete calculations, we should determine the parameters c_1 and c_2 in Eq. (4.1). Since there have no measurement of the dipion decays between different B_c states, we would fit these parameters from the bottomonium segment, which is the same as in Ref. [99]. Numerically, we take $|c_1|^2 = 61.8 \times 10^{-6}$ and $|c_2|^2 = 1.93 \times 10^{-6}$ [90] in the calculations.

With the above preparations, we calculate the decay rates of dipion transitions between B_c states. In Table 6, we present our results of the decay rates of dipion transitions $B_c(2S) \rightarrow B_c(1S)\pi^+\pi^-$, $B_c(2P) \rightarrow B_c(1P)\pi^+\pi^-$, and $B_c(1D) \rightarrow B_c(1S)\pi^+\pi^-$. We notice the discrepancies between the

Table 6 Decay rates of dipion transitions between B_c states. Here, the decay rates are given in units of keV

Initial states	Final states	This work	GI [52]	Ref. [99]
2^1S_0	$1^1S_0 + \pi^+\pi^-$	25	57	42
2^3S_1	$1^3S_1 + \pi^+\pi^-$	21	57	41
2^3P_0	$1^3P_0 + \pi^+\pi^-$	2.8	0.97	12
	$1^3P_2 + \pi^+\pi^-$	1.2×10^{-4}	0.055	5.5×10^{-3}
	$1P_1 + \pi^+\pi^-$	0	0	0
	$1P'_1 + \pi^+\pi^-$	0	0	0
2^3P_2	$1^3P_0 + \pi^+\pi^-$	5.7×10^{-3}	0.011	0.018
	$1^3P_2 + \pi^+\pi^-$	3.0	1.0	11
	$1P_1 + \pi^+\pi^-$	2.7×10^{-3}	0.021	0.02
	$1P'_1 + \pi^+\pi^-$	9.7×10^{-4}	4.0×10^{-3}	
$2P_1$	$1^3P_0 + \pi^+\pi^-$	0	0	0
	$1^3P_2 + \pi^+\pi^-$	6.3×10^{-4}	0.037	0.012
	$1P_1 + \pi^+\pi^-$	1.5	2.7	11
	$1P'_1 + \pi^+\pi^-$	0.77	0.020	
$2P'_1$	$1^3P_0 + \pi^+\pi^-$	0	0	0
	$1^3P_2 + \pi^+\pi^-$	2.7×10^{-4}	4.0×10^{-3}	
	$1P_1 + \pi^+\pi^-$	1.4	0.10	
	$1P'_1 + \pi^+\pi^-$	1.6	1.2	11
1^3D_1	$1^3S_1 + \pi^+\pi^-$	0.15	4.3	0.75
1^3D_3	$1^3S_1 + \pi^+\pi^-$	0.23	4.3	0.84
$1D_2$	$1^1S_0 + \pi^+\pi^-$	0.20	2.1	
	$1^3S_1 + \pi^+\pi^-$	0.066	2.2	
$1D'_2$	$1^1S_0 + \pi^+\pi^-$	0.12	2.2	
	$1^3S_1 + \pi^+\pi^-$	0.13	2.1	

results from this work and Refs. [52,99]. In fact, there are also notable differences between the results from the GI model [52,99]. But, we still find some consistent conclusions for the decay rates, i.e., (i) For the $B_c(2S) \rightarrow B_c(1S)\pi^+\pi^-$ transitions, although our results are about a half of those of Refs. [52,99], but our result is comparable to those of the other two theoretical groups. Thus, we come to the same conclusion about the decay rates for these transitions, which are sizable. (ii) For the $B_c(2P) \rightarrow B_c(1P)\pi^+\pi^-$ transitions, our results show that $B_c(2^3P_0) \rightarrow B_c(1^3P_0)\pi^+\pi^-$, $B_c(2^3P_2) \rightarrow B_c(1^3P_2)\pi^+\pi^-$, $B_c(2P_1) \rightarrow B_c(1P_1)\pi^+\pi^-$, $B_c(2P_1) \rightarrow B_c(1P'_1)\pi^+\pi^-$, $B_c(2P'_1) \rightarrow B_c(1P_1)\pi^+\pi^-$, and $B_c(2P'_1) \rightarrow B_c(1P'_1)\pi^+\pi^-$ have significant decay rates and other transitions are suppressed. In general, this conclusion was supported by the GI model [52,99]. (iii) Regarding the $B_c(1D) \rightarrow B_c(1S)\pi^+\pi^-$ transitions, it is noteworthy that our result is an order of magnitude smaller than the corresponding result from the GI model [52], but comparable to that of Ref. [99], taking $B_c(1^3D_1) \rightarrow B_c(1^3S_1)\pi^+\pi^-$ and $B_c(1^3D_3) \rightarrow B_c(1^3S_1)\pi^+\pi^-$ as examples. Obviously, the study of these dipion transitions of B_c mesons should be further pursued both theoretically and experimentally.

In addition to focusing on the decay rates of these dipion transitions of B_c mesons, we should also pay more attention to their dipion mass distributions, which are also accessible in experiment. Taking some dipion transitions of heavy quarkonia as an example, we find that the experiment already reported the dipion mass distributions of $\psi(3686) \rightarrow J/\psi\pi^+\pi^-$ [100], $\psi(3770) \rightarrow J/\psi\pi^+\pi^-$ [101], $\Upsilon(2S, 3S, 4S) \rightarrow \Upsilon(1S)\pi^+\pi^-$ [102–104], and so on. The QCDME approach can reproduce well the line shape of the dipion mass distribution of the dipion transitions of some low-lying heavy quarkonia such as $\psi(3686) \rightarrow J/\psi\pi^+\pi^-$ and $\Upsilon(2S) \rightarrow \Upsilon(1S)\pi^+\pi^-$ [88]. However, for higher heavy quarkonia near or above the threshold of the OZI-allowed hadronic channel, it is difficult to directly apply the QCDME approach to describe the corresponding dipion mass distribution [94,105–107], since the QCDME approach is a typical quenched quark model. Usually, for higher heavy quarkonia, the unquenched effects become important [89,94,105–122].

In this work, we hope to provide the dipion mass distributions of some discussed dipion transitions of B_c mesons, which are shown in Fig. 3. We want to emphasize that the

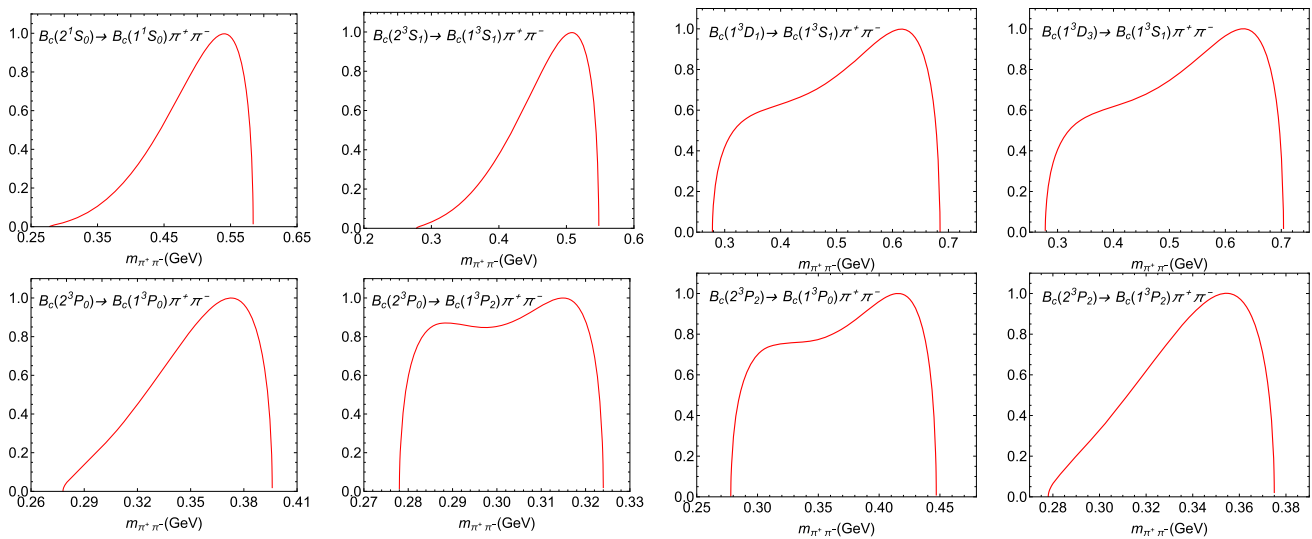


Fig. 3 The dipion invariant mass spectrum distributions of $B_c(2^1S_0) \rightarrow B_c(1^1S_0)\pi^+\pi^-$ and $B_c(2^3S_1) \rightarrow B_c(1^3S_1)\pi^+\pi^-$, and $B_c(2^3P_0) \rightarrow B_c(1^3P_0)\pi^+\pi^-$ and $B_c(2^3P_2) \rightarrow B_c(1^3P_{0(2)})\pi^+\pi^-$,

and $B_c(1^3D_{1(3)}) \rightarrow B_c(1^3S_1)\pi^+\pi^-$ processes. Here, we have normalized the maxima of the dipion distributions to 1

maxima of dipion mass distributions are all normalized to 1, since we only concern on their line shapes. Here, we not only select some decays of low-lying B_c mesons far below the BD threshold, i.e., $B_c(2^3S_1) \rightarrow B_c(1^3S_1)\pi^+\pi^-$ and $B_c(2^1S_0) \rightarrow B_c(1^1S_0)\pi^+\pi^-$, but also take some decays of B_c mesons above (or near) the BD threshold, like $B_c(2^3P_0) \rightarrow B_c(1^3P_{0(2)})\pi^+\pi^-$, $B_c(2^3P_2) \rightarrow B_c(1^3P_{0(2)})\pi^+\pi^-$, and $B_c(1^3D_{1(3)}) \rightarrow B_c(1^3S_1)\pi^+\pi^-$. At the present, this experimental information is still missing. Therefore, we strongly suggest our experimental colleagues to carry out the measurement of the dipion mass distributions of the B_c dipion transitions, which is sensitive to reflect the difference in the result under the quenched and unquenched pictures.

5 Radiative decays and magnetic moments

In this section, we will delve into the electric dipole (E1) and magnetic dipole (M1) radiative decay behaviors and the magnetic moments exhibited by the relevant B_c states. These observations hold significant implications for unraveling their intricate internal structures.

5.1 The E1 transitions

To commence our explorations, we will delve into the E1 transition decays of the aforementioned B_c states. The partial widths associated with the E1 radiative transition in the nonrelativistic quark model can be obtained using the fol-

lowing expression [123, 124]

$$\Gamma(i \rightarrow f + \gamma) = \frac{4}{3} \langle e_Q \rangle^2 \alpha \omega^3 C_{fi} \delta_{SS'} |\langle f | r | i \rangle|^2 \tag{5.1}$$

with

$$C_{fi} = \text{Max}(L, L') (2J' + 1) \left\{ \begin{matrix} L' & J' & S \\ J & L & 1 \end{matrix} \right\}^2, \tag{5.2}$$

$$\langle e_Q \rangle = \frac{m_b e_c - m_c e_{\bar{b}}}{m_b + m_c}. \tag{5.3}$$

Additionally, we denote m_c and m_b as the masses of the charm and bottom quarks, respectively. The corresponding charges of the charm and bottom quarks are $e_c = 2/3$ and $e_b = -1/3$, respectively. The energy of the photon, denoted as ω , can be obtained through the conservation of energy and momentum, expressed as follows:

$$M_i = \sqrt{M_f^2 + \omega^2} + \omega, \tag{5.4}$$

where M_i and M_f are the masses of the parent and daughter mesons, respectively.

In Table 7, we present the widths of electric dipole decays for the discussed B_c states and compare them with those obtained from other models. Upon scrutinizing the results in Table 7, we observe that the overall magnitude of our calculations remains below 0.1 MeV, which is several orders of magnitude smaller than the two-body OZI-allowed strong decays calculated earlier. Given the limited availability of experimental data, we can only discuss our findings in relation to other theoretical predictions. When comparing our

Table 7 Widths of the E1 transitions for the 1*P*-wave, 1*D*-wave, 1*F*-wave, 2*S*-wave, 2*P*-wave, and 3*S*-wave *B_c* states compared with those from other theoretical work. Here, the width is in units of keV

Initial states	Final states	This work	GI [52]	Ref. [51]	Ref. [49]	Initial states	Final states	This work	GI [52]	Ref. [51]	Ref. [49]
1 ³ <i>P</i> ₀	1 ³ <i>S</i> ₁ γ	52.3	55	67	65	2 ³ <i>P</i> ₀	1 ³ <i>S</i> ₁ γ	0.4	1.0		16.1
1 ³ <i>P</i> ₂	1 ³ <i>S</i> ₁ γ	85.1	83	107	103		2 ³ <i>S</i> ₁ γ	33.6	42	29	26
1 <i>P</i> ' ₁	1 ¹ <i>S</i> ₀ γ	64.0	80	132	11		1 ³ <i>D</i> ₁ γ	2.4	4.2	0.036	3.2
	1 ³ <i>S</i> ₁ γ	25.6	11	14	8.1	2 ³ <i>P</i> ₂	1 ³ <i>S</i> ₁ γ	15.5	14		19
1 <i>P</i> ₁	1 ¹ <i>S</i> ₀ γ	30.1	13	18	12		2 ³ <i>S</i> ₁ γ	48.9	55	57	49
	1 ³ <i>S</i> ₁ γ	47.8	60	79	78		1 ³ <i>D</i> ₁ γ	0.08	0.10	0.035	0.1
1 ³ <i>D</i> ₁	1 ³ <i>P</i> ₀ γ	53.8	55	128	80		1 ³ <i>D</i> ₃ γ	5.4	6.8	1.6	11
	1 ³ <i>P</i> ₂ γ	1.7	1.8	5.5	2.2		1 <i>D</i> ' ₂ γ	0.6	0.70	0.11	0.5
	1 <i>P</i> ' ₁ γ	9.1	4.4	7.7	3.3		1 <i>D</i> ₂ γ	0.4	0.60	0.27	1.5
	1 <i>P</i> ₁ γ	21.2	28	74	39	2 <i>P</i> ' ₁	1 ¹ <i>S</i> ₀ γ	14.6	19		
1 ³ <i>D</i> ₃	1 ³ <i>P</i> ₂ γ	74.6	78	102	75		2 ¹ <i>S</i> ₀ γ	42.4	52		
1 <i>D</i> ' ₂	1 ³ <i>P</i> ₂ γ	11.7	8.8	13	6.8		1 ³ <i>S</i> ₁ γ	1.0	0.6		
	1 <i>P</i> ' ₁ γ	74.2	63	116	46		2 ³ <i>S</i> ₁ γ	9.6	5.5		
	1 <i>P</i> ₁ γ	0.8	7	7.3	25		1 ³ <i>D</i> ₁ γ	0.3	0.2		
1 <i>D</i> ₂	1 ³ <i>P</i> ₂ γ	6.0	9.6	28	12		1 <i>D</i> ' ₂ γ	3.3	5.5		
	1 <i>P</i> ' ₁ γ	0.1	15	14	18		1 <i>D</i> ₂ γ	1.3	1.3		
	1 <i>P</i> ₁ γ	67.6	64	112	45	2 <i>P</i> ₁	1 ¹ <i>S</i> ₀ γ	3.5	2.1		
1 ³ <i>F</i> ₂	1 ³ <i>D</i> ₁ γ	68.2	75				2 ¹ <i>S</i> ₀ γ	9.7	5.7		
	1 ³ <i>D</i> ₃ γ	0.3	0.4				1 ³ <i>S</i> ₁ γ	3.8	5.4		
	1 <i>D</i> ' ₂ γ	6.9	6.3				2 ³ <i>S</i> ₁ γ	35.1	45		
	1 <i>D</i> ₂ γ	4.2	6.5				1 ³ <i>D</i> ₁ γ	1.1	1.6		
1 ³ <i>F</i> ₄	1 ³ <i>D</i> ₃ γ	70.6	81				1 <i>D</i> ' ₂ γ	0.5	0.8		
1 <i>F</i> ' ₃	1 ³ <i>D</i> ₃ γ	5.1	3.7				1 <i>D</i> ₂ γ	3.0	3.6		
	1 <i>D</i> ' ₂ γ	71.6	78			3 ¹ <i>S</i> ₀	1 <i>P</i> ' ₁ γ	3.0			
	1 <i>D</i> ₂ γ	0.6	0.5				1 <i>P</i> ₁ γ	1.6			
1 <i>F</i> ₃	1 ³ <i>D</i> ₃ γ	3.0	5.4				2 <i>P</i> ' ₁ γ	9.0			
	1 <i>D</i> ' ₂ γ	0.03	0.04				2 <i>P</i> ₁ γ	2.9			
	1 <i>D</i> ₂ γ	69.1	82			3 ³ <i>S</i> ₁	1 ³ <i>P</i> ₀ γ	0.04			
2 ¹ <i>S</i> ₀	1 <i>P</i> ' ₁ γ	4.4	6.1	3.7	16		1 ³ <i>P</i> ₂ γ	2.2			
	1 <i>P</i> ₁ γ	2.8	1.3	1.0	1.9		1 <i>P</i> ' ₁ γ	0.04			
2 ³ <i>S</i> ₁	1 ³ <i>P</i> ₀ γ	3.0	2.9	3.8	7.7		1 <i>P</i> ₁ γ	0.3			
	1 ³ <i>P</i> ₂ γ	5.3	5.7	5.2	15		2 ³ <i>P</i> ₀ γ	3.8			
	1 <i>P</i> ' ₁ γ	1.3	0.7	0.63	1.0		2 ³ <i>P</i> ₂ γ	7.6			
	1 <i>P</i> ₁ γ	3.6	4.7	5.1	13		2 <i>P</i> ' ₁ γ	1.2			
							2 <i>P</i> ₁ γ	5.8			

results with those obtained from the GI model [52], we find substantial agreement in most cases, with only a few discrepancies. These variations could potentially arise from the introduction of the screening effects, such as the transitions $B_c(1D'_2) \rightarrow B_c(1P_1)\gamma$, $B_c(1D_2) \rightarrow B_c(1P'_1)\gamma$, and so on.

Now let's delve into a detailed analysis of the obtained results presented in Table 7. Regarding the calculations for the initial state of 1*P*-wave, our findings exhibit consistency with the GI model [52], as well as with Refs. [49,51], and no instances of underestimation are observed. However, for the

cases involving initial states of 1*D*-wave and 1*F*-wave, we have noticed a systematic tendency toward underestimation in the results. We notice that these results for the processes $B_c(1^3D_1) \rightarrow B_c(1^3P_2)\gamma$, $B_c(1^3F_2) \rightarrow B_c(1^3D_3)\gamma$, and $B_c(1D'_2) \rightarrow B_c(1P_1)\gamma$, as well as $B_c(1F'_3) \rightarrow B_c(1D_2)\gamma$, $B_c(1D_2) \rightarrow B_c(1P'_1)\gamma$, and $B_c(1F_3) \rightarrow B_c(1D'_2)\gamma$, are underestimated. Upon closer examination of the transition processes listed above, we can discern a fascinating pattern: the underestimation occurs consistently across similar transition processes when transitioning from a higher-order excited

state to a lower-order excited state. Truly, this phenomenon is a remarkable finding.

5.2 The M1 transitions

We perform calculations and explore the M1 transition decays of the aforementioned B_c states. The M1 transition is frequently employed to investigate the radiative transition behavior of quarkonia. Since the B_c meson comprises an antibottom quark and a charm quark, its properties lie intermediate to those of charmonium and bottomonium. Consequently, we can leverage the formulas previously discussed for quarkonia to analyze the behavior of B_c mesons. The magnetic dipole transition width between quarkonium states is given by the following expression [123, 125]

$$\Gamma(i \rightarrow f + \gamma) = \frac{\alpha}{3} \mu^2 \omega^3 (2J_f + 1) \left| \left\langle f \left| j_0 \left(\frac{kr}{2} \right) \right| i \right\rangle \right|^2 \quad (5.5)$$

under the nonrelativistic approximation, where

$$\mu = \frac{e_c}{m_c} - \frac{e_{\bar{b}}}{m_{\bar{b}}}, \quad (5.6)$$

and $j_0(x)$ is the spherical Bessel function, i.e.,

$$j_0(x) = \frac{\sin x}{x}. \quad (5.7)$$

In Table 8, we present the magnetic dipole decay widths of the aforementioned B_c states. Upon examining the results, we observe that for a given initial state, the decay width increases as the principal quantum number n decreases. This finding aligns with the conclusions drawn by previous studies [52]. Conversely, for a fixed final state, the decay width decreases as the initial state's principal quantum number n increases. This intriguing phenomenon warrants further investigations. We have observed two transitions that exhibit significant suppression, which are $B_c(4^3S_1) \rightarrow B_c(4^1S_0)\gamma$ and $B_c(5^3S_1) \rightarrow B_c(5^1S_0)\gamma$, with corresponding values of 1.1 eV and 0.6 eV, respectively. Although experimental progress regarding the radiative transition behavior of B_c mesons remains elusive, we expect that our discussions on this topic will offer theoretical insights for future experimental explorations of B_c mesons and will prove valuable in this regard.

5.3 Magnetic moments

We delve into the magnetic moments of the discussed B_c states, which serve as essential and significant physical observables of hadrons. Magnetic moments are fundamental quantities that have garnered considerable attention and

sparked extensive discussions over the past decades, particularly in relation to the magnetic moments of the decuplet and octet baryons. Numerous theoretical models and approaches have been employed to investigate the magnetic moments of hadronic states, including the constituent quark model, the Bag model, the lattice QCD simulations, the chiral perturbation theory, the QCD sum rule, and others [12].

The magnetic moments of the B_c states can be calculated by the following expectation values [126–171]

$$\mu_{B_c} = \langle J_{B_c}, J_{B_c} | \hat{\mu}_z | J_{B_c}, J_{B_c} \rangle. \quad (5.8)$$

In the case of the B_c states, the spatial wave function fulfills the normalization condition, and the color wave function is unity due to the color confinement. Consequently, the magnetic moments of the B_c states are determined by their flavor and spin-orbit wave functions.

In this study, we employ the constituent quark model to explore the magnetic moments of the discussed B_c states. This approach is analogous to the investigations of the magnetic moments of the decuplet and octet baryons conducted in previous studies [126–128]. Within the framework of the constituent quark model, the total magnetic moment of the B_c state is composed of two distinct components: the spin magnetic moment and the orbital magnetic moment. The z -component of the spin magnetic moment operator, denoted as $\hat{\mu}_z^{\text{spin}}$, and the orbital magnetic moment operator, denoted as $\hat{\mu}_z^{\text{orbital}}$, can be expressed as [126–171]

$$\hat{\mu}_z^{\text{spin}} = \sum_{i=c,\bar{b}} \mu_i \hat{\sigma}_{iz}, \quad (5.9)$$

$$\hat{\mu}_z^{\text{orbital}} = \frac{m_c \mu_{\bar{b}}}{m_c + m_{\bar{b}}} \hat{L}_z + \frac{m_{\bar{b}} \mu_c}{m_c + m_{\bar{b}}} \hat{L}_z, \quad (5.10)$$

respectively. Here, $\mu_i = q_i/(2m_i)$ represents the magnetic moment of the i th quark, where q_i and m_i denote the charge and mass of the i th quark, respectively. Moreover, $\hat{\sigma}_{iz}$ corresponds to the Pauli spin operator associated with the i -th quark. In the context of the B_c meson, the subscripts c and \bar{b} refer to the charm quark and the antibottom quark, respectively. Additionally, \hat{L}_z represents the z -component of the orbital angular momentum operator between the c and \bar{b} quarks.

In the case of the S -wave B_c states, the contribution from the orbital magnetic moment is zero due to the absence of the orbital angular momentum ($L_z = 0$). Therefore, we only need to consider the contribution from the spin magnetic moment for the S -wave B_c states. On the other hand, for the orbital excited B_c states, the total magnetic moments comprise both the spin magnetic moment and the orbital magnetic moment. The spin-orbit wave function $|^{2S+1}L_J\rangle$ for the orbital excited B_c states can be expanded by coupling the orbital wave function Y_{L,m_L} with the spin wave function

Table 8 Partial widths of the M1 transitions for the S -wave B_c states compared with other theoretical works. Here, the width is in units of eV

Initial states	Final states	This work	GI [52]	Ref. [48]	Ref. [51]	Ref. [50]	
1^3S_1	$1^1S_0\gamma$	83.6	80	135	33	59	
2^3S_1	$2^1S_0\gamma$	8.3	10	29	17	12	
3^3S_1	$1^1S_0\gamma$	559.3	600	123	428	122	
	$3^1S_0\gamma$	2.2	3				
	$2^1S_0\gamma$	139.3	200				
4^3S_1	$1^1S_0\gamma$	503.7	600				
	$4^1S_0\gamma$	1.1					
	$3^1S_0\gamma$	62.2					
	$2^1S_0\gamma$	151.2					
5^3S_1	$1^1S_0\gamma$	443.0					
	$5^1S_0\gamma$	0.6					
	$4^1S_0\gamma$	34.8					
	$3^1S_0\gamma$	73.1					
	$2^1S_0\gamma$	146.5					
2^1S_0	$1^1S_0\gamma$	390.0					
	$1^3S_1\gamma$	320.6	300	93	488	59	
	3^1S_0	53.0	60				
	4^1S_0	$1^3S_1\gamma$	443.5	4200			
		$3^3S_1\gamma$	15.6				
$2^3S_1\gamma$		114.0					
5^1S_0	$1^3S_1\gamma$	452.2					
	$4^3S_1\gamma$	6.0					
	$3^3S_1\gamma$	45.6					
	$2^3S_1\gamma$	138.5					
	$1^3S_1\gamma$	431.5					

χ_{S,m_S} , resulting in the following expression [168]:

$$|^{2S+1}L_J\rangle = \sum_{m_L,m_S} C_{Lm_L,Sm_S}^{JM} Y_{L,m_L} \chi_{S,m_S}, \tag{5.11}$$

where C_{Lm_L,Sm_S}^{JM} is the Clebsch–Gordan coefficient. Here, we need to point out that the orbital magnetic moment and the spin magnetic moment can be obtained by sandwiching the orbital and spin magnetic moment operators between the relevant spin-orbit and flavor wave functions.

To illustrate the calculations of magnetic moments for the orbital excited B_c states, let us consider the nP -wave B_c states, which include the $B_c(n^3P_0)$, $B_c(n^3P_1)$, $B_c(n^1P_1)$, and $B_c(n^3P_2)$ states. In this case, due to the mixture of the spin-singlet and spin-triplet states, it is necessary to expand their spin-orbital wave functions $|^{2S+1}L_J\rangle$ as follows:

$$\begin{aligned} |n^3P_0\rangle &= \frac{1}{\sqrt{3}}Y_{1,-1}\chi_{1,1} - \frac{1}{\sqrt{3}}Y_{1,0}\chi_{1,0} + \frac{1}{\sqrt{3}}Y_{1,1}\chi_{1,-1}, \\ |n^3P_1\rangle &= \frac{1}{\sqrt{2}}Y_{1,1}\chi_{1,0} - \frac{1}{\sqrt{2}}Y_{1,0}\chi_{1,1}, \\ |n^1P_1\rangle &= Y_{1,1}\chi_{0,0}, \end{aligned}$$

$$|n^3P_2\rangle = Y_{1,1}\chi_{1,1}. \tag{5.12}$$

Using the previously expanded spin-orbital wave functions, we can proceed to calculate the magnetic moments and the transition magnetic moments of the nP -wave B_c states. The explicit expressions for these quantities are

$$\begin{aligned} \mu_{B_c(n^3P_0)} &= 0, \\ \mu_{B_c(n^3P_1)} &= \frac{1}{2}\mu_c + \frac{1}{2}\mu_{\bar{b}} + \frac{1}{2}\mu_{c\bar{b}}^L, \\ \mu_{B_c(n^1P_1)} &= \mu_{c\bar{b}}^L, \\ \mu_{B_c(n^3P_2)} &= \mu_c + \mu_{\bar{b}} + \mu_{c\bar{b}}^L, \\ \mu_{B_c(n^3P_1) \rightarrow B_c(n^1P_1)} &= \frac{1}{\sqrt{2}}\mu_c - \frac{1}{\sqrt{2}}\mu_{\bar{b}}, \end{aligned} \tag{5.13}$$

where we introduce the notation $\mu_{c\bar{b}}^L = \frac{m_c\mu_{\bar{b}}}{m_c+m_{\bar{b}}} + \frac{m_b\mu_c}{m_c+m_{\bar{b}}}$ to simplify the magnetic moment calculations. It is important to note that the calculation method for the transition magnetic moments between the nP -wave B_c states is similar to that of the magnetic moments of the nP -wave B_c states, with the only difference being the wave functions of the initial and final states. For a more detailed calculation of the transition

magnetic moments, please refer to Refs. [129–131, 140, 146, 148, 152, 154–159, 162, 166–168].

For the nP -wave B_c states, it is important to consider the mixing of the $B_c(n^1P_1)$ and $B_c(n^3P_1)$ states, as discussed in Sect. 2. Referring to Eq. (2.10), we can obtain the following expressions:

$$\begin{aligned} |nP'_1\rangle &= |n^1P_1\rangle \cos\theta_{nP} + |n^3P_1\rangle \sin\theta_{nP}, \\ |nP_1\rangle &= -|n^1P_1\rangle \sin\theta_{nP} + |n^3P_1\rangle \cos\theta_{nP}. \end{aligned} \tag{5.14}$$

Here, θ_{nP} represents the mixing angle between the $B_c(n^1P_1)$ and $B_c(n^3P_1)$ states, as provided in Table 3. With these preparations, we can proceed to calculate the magnetic moments of the mixed states of the $B_c(n^1P_1)$ and $B_c(n^3P_1)$ states. The magnetic moments of these mixed states can be calculated using the following relations:

$$\begin{aligned} \mu_{B_c(nP'_1)} &= \mu_{|n^1P_1\rangle} \cos^2\theta_{nP} + \mu_{|n^3P_1\rangle \rightarrow |n^1P_1\rangle} \sin 2\theta_{nP} \\ &\quad + \mu_{|n^3P_1\rangle} \sin^2\theta_{nP}, \\ \mu_{B_c(nP_1)} &= \mu_{|n^1P_1\rangle} \sin^2\theta_{nP} - \mu_{|n^3P_1\rangle \rightarrow |n^1P_1\rangle} \sin 2\theta_{nP} \\ &\quad + \mu_{|n^3P_1\rangle} \cos^2\theta_{nP}. \end{aligned} \tag{5.15}$$

Therefore, the magnetic moments of the mixed states of the $B_c(n^1P_1)$ and $B_c(n^3P_1)$ states are determined not only by the magnetic moments and the transition magnetic moments of the $B_c(n^1P_1)$ and $B_c(n^3P_1)$ states but also by the mixing angles of the $B_c(n^1P_1)$ and $B_c(n^3P_1)$ states.

Within the framework of the constituent quark model, the masses of the involved quarks play a crucial role in the study of their magnetic moment properties. In our calculations, we adopt the quark masses $m_c = 1.660$ GeV and $m_b = 4.730$ GeV, which have been widely used to describe the hadronic magnetic moments quantitatively [133, 167, 172–176]. Table 9 presents the magnetic moments of the $S/P/D/F$ -wave B_c mesons obtained from our calculations. Furthermore, we compare our results with those from other theoretical works and find that our findings are in good agreement with the theoretical predictions in Ref. [167]. It is important to note that the investigations of the magnetic moments of B_c states have not received much attention thus far. Therefore, we hope that our work will stimulate further theoretical and experimental efforts to explore the magnetic moments of the B_c states.

As widely acknowledged, phenomena in the higher mass region are highly intricate. This domain encompasses various conventional B_c states, which possess identical quantum numbers and similar masses, as well as predicted B_c -like molecular states [178]. Distinguishing between these states poses a critical challenge for both theoretical and experimental aspects. For instance, consider the conventional $B_c(2P'_1)$ state and the DB^* molecular state with $I(J^P) = 0(1^+)$, which have closely aligned masses. However, it has been observed that their magnetic moments exhibit evident differ-

Table 9 Magnetic moments of the $S/P/D/F$ -wave B_c mesons. Here, the magnetic moment of the hadron is in units of the nuclear magneton $\mu_N = e/2m_p$

States	Expressions	Results	Ref. [167]	Ref. [177]
1S_0	0	0	0	0
3S_1	$\mu_c + \mu_{\bar{b}}$	0.443		0.350
3P_0	0	0	0	
3P_2	$\mu_c + \mu_{\bar{b}} + \mu_{cb}^L$	0.739	0.739	
$1P'_1$		0.527		
$1P_1$		0.138		
$2P'_1$		0.486	0.437	
$2P_1$		0.179	0.229	
$3P'_1$		0.469	0.454	
$3P_1$		0.197		
$4P'_1$		0.460		
$4P_1$		0.205		
3D_1	$-\frac{1}{2}(\mu_c + \mu_{\bar{b}}) + \frac{3}{2}\mu_{cb}^L$	0.223		
3D_3	$\mu_c + \mu_{\bar{b}} + 2\mu_{cb}^L$	1.035		
$1D'_2$		0.381		
$1D_2$		0.852		
$2D'_2$		0.368		
$2D_2$		0.865		
$2D'_2$		0.362		
$3D_2$		0.871		
3F_2	$-\frac{2}{3}(\mu_c + \mu_{\bar{b}}) + \frac{8}{3}\mu_{cb}^L$	0.494		
3F_4	$\mu_c + \mu_{\bar{b}} + 3\mu_{cb}^L$	1.331		
$1F'_3$		0.646		
$1F_3$		1.167		
$2F'_3$		0.644		
$2F_3$		1.169		

ences, i.e., $\mu_{B_c(2P'_1)} = 0.486\mu_N$, $\mu_{DB^*[0(1^+)]} = 0.532\mu_N$ [167]. There are many such examples. Consequently, investigating the magnetic moment properties provides a means to differentiate between states sharing identical quantum numbers and similar masses.

6 Some typical weak decays of the $B_c(1^3S_0)$ meson

As the lowest bottom-charmed meson, the $B_c(1^3S_0)$ meson can only decay via the weak process. For simplicity, we use B_c to denote the $B_c(1^3S_0)$ in this section. In experiments, a series weak processes have been observed, while the absolute branching ratios are deficiency for most of them [46]. Previous theoretical studies on B_c weak decays have been conducted using lattice QCD (LQCD) [179, 180], perturbative QCD [181, 182], QCD sum rule [183, 184], light-cone sum rule [185], various quark models [186–198], and other meth-

ods [199]. With the updated high luminosity of the LHC, the experimental measurements of these weak decays become feasible, and this will demand more theoretical studies.

In theoretical aspects, the light-front quark model is a powerful phenomenological model to calculate the weak transition matrix elements of mesons and baryons decays. Specially, the B_c weak decays have been studied by the CLFQM in Refs. [191–198]. However, in the concrete calculations, the important input, i.e., the spatial wave function, is usually adopted as the Gaussian-like form, and may bring large uncertainty due to the phenomenological parameter β . In this work, we also employ the CLFQM to revisit the B_c weak decays. In our calculations, we adopt the numerical spatial wave functions of the involved mesons, which benefit from the MGI model introduced in Sect. 2, as opposed to SHO wave functions with a phenomenological parameter β used in previous works based on the CLFQM [191–198]. This approach reduces the dependence on phenomenological parameters in determining the form factors.

In order to make a comprehensive discussion, we first discuss the $B_c \rightarrow M$ weak transition form factors, where M represents a pseudoscalar meson (P), vector meson (V), scalar meson (S), or axial meson (A). These transitions involve the quark-level transitions $b \rightarrow c(u)$ and $c \rightarrow s(d)$. Additionally, we employ these form factors as inputs to investigate various weak decays, including semileptonic decays and typical two-body nonleptonic decays.

Generally, the $B_c \rightarrow M$ transitions induced by the $V - A$ current can be expressed as [200]

$$\begin{aligned}
 \langle P(p'')|V_\mu|B_c(p')\rangle &= \left(P_\mu - \frac{m_{B_c}^2 - m_P^2}{q^2}q_\mu\right)F_1^{B_c P}(q^2) \\
 &\quad + \frac{m_{B_c}^2 - m_P^2}{q^2}q_\mu F_0^{B_c P}(q^2), \\
 \langle V(p'')|V_\mu|B_c(p')\rangle &= -\frac{1}{m_{B_c} + m_V}\epsilon_{\mu\nu\alpha\beta}\epsilon_V^{*\nu}P^\alpha q^\beta V^{B_c V}(q^2), \\
 \langle V(p'')|A_\mu|B_c(p')\rangle &= i\left\{(m_{B_c} + m_V)\epsilon_{V\mu}^*A_1^{B_c V}(q^2) \right. \\
 &\quad \left. - \frac{\epsilon_V^* \cdot P}{m_{B_c} + m_V}P_\mu A_2^{B_c V}(q^2) - 2m_V \frac{\epsilon_V^* \cdot P}{q^2}q_\mu \left[A_3^{B_c V}(q^2) - A_0^{B_c V}(q^2)\right]\right\}, \\
 \langle A(p'')|V_\mu|B_c(p')\rangle &= -i\left\{(m_{B_c} - m_A)\epsilon_{A\mu}^*V_1^{B_c A}(q^2) - \frac{\epsilon_A^* \cdot P}{m_{B_c} - m_A} \right. \\
 &\quad \left. P_\mu V_2^{B_c A}(q^2) - 2m_A \frac{\epsilon_A^* \cdot P}{q^2}q_\mu \left[V_3^{B_c A}(q^2) - V_0^{B_c A}(q^2)\right]\right\}, \\
 \langle A(p'')|A_\mu|B_c(p')\rangle &= -\frac{1}{m_{B_c} - m_A}\epsilon_{\mu\nu\alpha\beta}\epsilon_A^{*\nu}P^\alpha q^\beta A^{B_c A}(q^2), \\
 \langle S(p'')|A_\mu|B_c(p')\rangle &= \left(P_\mu - \frac{m_{B_c}^2 - m_S^2}{q^2}q_\mu\right)F_1^{B_c S}(q^2) \\
 &\quad + \frac{m_{B_c}^2 - m_S^2}{q^2}q_\mu F_0^{B_c S}(q^2), \tag{6.1}
 \end{aligned}$$

where p' and p'' are the momenta of the initial state meson B_c and the final state meson $P/V/A/S$, respectively. Besides,

we define $P_\mu = p'_\mu + p''_\mu$ and $q_\mu = p'_\mu - p''_\mu$, while the convention $\epsilon_{0123} = +1$ is used.

In the frame of the CLFQM, the constituent (anti)quark inside a meson system are off-shell. The parent and daughter mesons have the four momenta $P' = p'_1 + p_2$ and $P'' = p''_1 + p_2$, where $p_1^{(i)}$ and p_2 are the four momenta of the quark and the antiquark, respectively. These momenta can be expressed in terms of the following internal variables (x_i, \vec{k}'_\perp) ($i = 1, 2$):

$$p_1^{'+} = x_1 P'^+, \quad p_1^+ = x_2 P'^+, \quad \vec{p}'_{1\perp} = x_1 \vec{P}'_\perp + \vec{k}'_\perp, \tag{6.2}$$

where they must satisfy the relation $x_1 + x_2 = 1$.

The $B_c \rightarrow M$ weak transition form factors have been widely studied by CLFQM in Refs. [191–197]. As derived in Refs. [192, 195, 197, 201–203], the $B_c \rightarrow P$ weak transition form factors are

$$\begin{aligned}
 F_1^{B_c P}(q^2) &= \frac{N_c}{16\pi^3} \int dx_2 d^2\vec{k}'_\perp \frac{h'_{B_c} h''_P}{x_2 \hat{N}'_1 \hat{N}''_1} \left[x_1 (M_0^2 + M_0''^2) + x_2 q^2 \right. \\
 &\quad \left. - x_2 (m'_1 - m''_1)^2 - x_1 (m'_1 - m_2)^2 - x_1 (m''_1 - m_2)^2 \right], \tag{6.3}
 \end{aligned}$$

$$\begin{aligned}
 F_0^{B_c P}(q^2) &= F_1^{B_c P}(q^2) + \frac{q^2}{P \cdot q} \frac{N_c}{16\pi^3} \int dx_2 d^2\vec{k}'_\perp \frac{2h'_{B_c} h''_P}{x_2 \hat{N}'_1 \hat{N}''_1} \\
 &\quad \times \left\{ -x_1 x_2 M^2 - k_\perp^2 - m'_1 m_2 + (m'_1 - m_2) \right. \\
 &\quad \times (x_2 m'_1 + x_1 m_2) + 2 \frac{P \cdot q}{q^2} (k_\perp^2 + 2 \frac{(\vec{k}'_\perp \cdot \vec{q}_\perp)^2}{q^2}) \\
 &\quad + 2 \frac{(\vec{k}'_\perp \cdot \vec{q}_\perp)^2}{q^2} - \frac{\vec{k}'_\perp \cdot \vec{q}_\perp}{q^2} \left[M''^2 - x_2 (q^2 + P \cdot q) \right. \\
 &\quad \left. \left. - (x_2 - x_1) M^2 + 2x_1 M_0^2 - 2(m'_1 - m_2)(m'_1 + m''_1) \right] \right\}, \tag{6.4}
 \end{aligned}$$

where

$$\begin{aligned}
 h'_{B_c} &= (M^2 - M_0^2) \sqrt{\frac{x_1 x_2}{N_c}} \frac{1}{\sqrt{2} \tilde{M}'_0} \phi_s(x_2, \vec{k}'_\perp), \\
 h''_P &= (M''^2 - M_0''^2) \sqrt{\frac{x_1 x_2}{N_c}} \frac{1}{\sqrt{2} \tilde{M}''_0} \phi_s(x_2, \vec{k}'_\perp) \tag{6.5}
 \end{aligned}$$

with

$$\begin{aligned}
 M_0^{i(\prime\prime)2} &= \frac{\vec{k}'_{\perp i(\prime\prime)2} + m_{i(\prime\prime)1}^2}{x_1} + \frac{\vec{k}'_{\perp i(\prime\prime)2} + m_{i(\prime\prime)2}^2}{x_2}, \\
 \tilde{M}_0^{i(\prime\prime)} &= \sqrt{M_0^{i(\prime\prime)2} - (m_{i(\prime\prime)1} - m_2)^2}, \\
 \vec{k}'_{\perp i(\prime\prime)} &= \vec{k}'_\perp - x_2 \vec{q}_\perp. \tag{6.6}
 \end{aligned}$$

Analogously, the $B_c \rightarrow S$ weak transition form factors are written as [193, 195, 197, 202, 203]

$$\begin{aligned}
 F_1^{B_c S}(q^2) &= \frac{N_c}{16\pi^3} \int dx_2 d^2\vec{k}'_\perp \frac{h'_{B_c} h''_S}{x_2 \hat{N}'_1 \hat{N}''_1} \left[x_1 (M_0^2 + M_0''^2) + x_2 q^2 \right. \\
 &\quad \left. - x_2 (m'_1 + m''_1)^2 - x_1 (m'_1 - m_2)^2 - x_1 (m''_1 + m_2)^2 \right], \tag{6.7}
 \end{aligned}$$

$$\begin{aligned}
 F_0^{B_c S}(q^2) &= F_1^{B_c S}(q^2) + \frac{q^2}{P \cdot q} \frac{N_c}{16\pi^3} \int dx_2 d^2 \vec{k}_\perp \frac{2h'_{B_c} h''_S}{x_2 \hat{N}'_1 \hat{N}''_1} \\
 &\times \left\{ -x_1 x_2 M^2 - \vec{k}_\perp^2 - m'_1 m_2 - (m''_1 + m_2) \right. \\
 &\times (x_2 m'_1 + x_1 m_2) + 2 \frac{P \cdot q}{q^2} (\vec{k}'_\perp \cdot \vec{q}_\perp)^2 \\
 &+ 2 \frac{(\vec{k}'_\perp \cdot \vec{q}_\perp)^2}{q^2} - \frac{\vec{k}'_\perp \cdot \vec{q}_\perp}{q^2} [M'^2 - x_2(q^2 + P \cdot q) \\
 &\left. - (x_2 - x_1)M^2 + 2x_1 M_0^2 - 2(m'_1 - m_2)(m'_1 - m''_1)] \right\}, \tag{6.8}
 \end{aligned}$$

where

$$h''_S = (M'^2 - M_0'^2) \sqrt{\frac{x_1 x_2}{N_c}} \frac{1}{\sqrt{2} \tilde{M}_0''} \frac{\tilde{M}_0''}{2\sqrt{3} M_0''} \phi_p(x_2, \vec{k}'_\perp). \tag{6.9}$$

The $B_c \rightarrow V$ transition form factors can be evaluated by

$$\begin{aligned}
 V^{B_c V} &= -(m_{B_c} + m_V)g, \\
 A_1^{B_c V} &= -f/(m_{B_c} + m_V), \quad A_2^{B_c V} = (m_{B_c} + m_V)a_+, \tag{6.10} \\
 A_0^{B_c V} &= \frac{m_{B_c} + m_V}{2m_V} A_1^{B_c V} - \frac{m_{B_c} - m_V}{2m_V} A_2^{B_c V} - \frac{q^2}{2m_V} a_-,
 \end{aligned}$$

where g, f, a_+ , and a_- are the scalar functions of q^2 . Their expressions in CLFQM are [191, 192, 195, 197, 201–203]

$$\begin{aligned}
 g(q^2) &= -\frac{N_c}{16\pi^3} \int dx_2 d^2 \vec{k}_{2\perp} \frac{2h'_{B_c} h''_V}{x_2 \hat{N}'_1 \hat{N}''_1} \\
 &\times \left\{ x_2 m'_1 + x_1 m_2 + (m'_1 - m''_1) \frac{\vec{k}'_\perp \cdot \vec{q}_\perp}{q^2} \right. \\
 &\left. + \frac{2}{\omega''_V} \left[\vec{k}'_\perp{}^2 + \frac{(\vec{k}'_\perp \cdot \vec{q}_\perp)^2}{q^2} \right] \right\}, \tag{6.11}
 \end{aligned}$$

$$\begin{aligned}
 f(q^2) &= \frac{N_c}{16\pi^3} \int dx_2 d^2 \vec{k}_\perp \frac{h'_{B_c} h''_V}{x_2 \hat{N}'_1 \hat{N}''_1} \\
 &\times \left\{ 2x_1(m_2 - m'_1)(M_0^2 + M_0'^2) - 4x_1 m''_1 M_0^2 + 2x_2 m'_1 P \cdot q \right. \\
 &+ 2m_2 q^2 - 2x_1 m_2(M^2 + M'^2) + 2(m'_1 - m_2)(m'_1 + m''_1)^2 \\
 &+ 8(m'_1 - m_2) \left[\vec{k}'_\perp{}^2 + \frac{(\vec{k}'_\perp \cdot \vec{q}_\perp)^2}{q^2} \right] \\
 &+ 2(m'_1 + m''_1)(q^2 + P \cdot q) \frac{\vec{k}'_\perp \cdot \vec{q}_\perp}{q^2} \\
 &- 4 \frac{q^2 \vec{k}'_\perp{}^2 + (\vec{k}'_\perp \cdot \vec{q}_\perp)^2}{q^2 \omega''_V} \\
 &\times \left[2x_1(M^2 + M_0^2) - q^2 - P \cdot q \right. \\
 &- 2(q^2 + P \cdot q) \frac{\vec{k}'_\perp \cdot \vec{q}_\perp}{q^2} - 2(m'_1 \\
 &\left. - m''_1)(m'_1 - m_2) \right\}, \tag{6.12}
 \end{aligned}$$

$$\begin{aligned}
 a_+(q^2) &= \frac{N_c}{16\pi^3} \int dx_2 d^2 \vec{k}_\perp \frac{2h'_{B_c} h''_V}{x_2 \hat{N}'_1 \hat{N}''_1} \\
 &\times \left\{ (x_1 - x_2)(x_2 m'_1 + x_1 m_2) - [2x_1 m_2 + m''_1 + (x_2 - x_1)m'_1] \right. \\
 &\frac{\vec{k}'_\perp \cdot \vec{q}_\perp}{q^2} - 2 \frac{x_2 q^2 + \vec{k}'_\perp \cdot \vec{q}_\perp}{x_2 q^2 \omega''_V} \\
 &\left. \times [\vec{k}'_\perp \cdot \vec{q}_\perp + (x_1 m_2 + x_2 m'_1)(x_1 m_2 - x_2 m''_1)] \right\}, \tag{6.13}
 \end{aligned}$$

$$\begin{aligned}
 a_-(q^2) &= \frac{N_c}{16\pi^3} \int dx_2 d^2 \vec{k}_\perp \frac{h'_{B_c} h''_V}{x_2 \hat{N}'_1 \hat{N}''_1} \\
 &\times \left\{ 2(2x_1 - 3)(x_2 m'_1 + x_1 m_2) - 8(m'_1 - m_2) \left[\frac{\vec{k}'_\perp{}^2}{q^2} \right. \right. \\
 &\left. \left. + 2 \frac{(\vec{k}'_\perp \cdot \vec{q}_\perp)^2}{q^4} \right] \right. \\
 &- [(14 - 12x_1)m'_1 - 2m''_1 - (8 - 12x_1)m_2] \frac{\vec{k}'_\perp \cdot \vec{q}_\perp}{q^2} \\
 &+ \frac{4}{\omega''_V} \left[(M^2 + M'^2 - q^2 + 2(m'_1 - m_2)(m''_1 + m_2)) \right. \\
 &\times (A_3^2 + A_4^{(2)} - A_2^1) + Z_2(3A_2^{(1)} - 2A_4^{(2)} - 1) \\
 &+ \frac{1}{2} P \cdot q (A_1^{(1)} + A_2^{(1)} - 1) [x_1(q^2 + P \cdot q) \\
 &- 2M'^2 - 2\vec{k}'_\perp \cdot \vec{q}_\perp \\
 &- 2m'_1(m''_1 + m_2 - 2m_2(m'_1 - m_2))] \\
 &\left. \left. \times \left[\frac{\vec{k}'_\perp{}^2}{q^2} + \frac{(\vec{k}'_\perp \cdot \vec{q}_\perp)^2}{q^4} \right] (4A_2^{(1)} - 3) \right] \right\}, \tag{6.14}
 \end{aligned}$$

where

$$\begin{aligned}
 h''_V &= (M'^2 - M_0'^2) \sqrt{\frac{x_1 x_2}{N_c}} \frac{1}{\sqrt{2} \tilde{M}_0''} \phi_s(x_2, \vec{k}'_\perp), \tag{6.15} \\
 \omega''_V &= M_0'' + m''_1 + m_2.
 \end{aligned}$$

For the $B_c \rightarrow {}^3A(^1A)$ transition, the form factors can be evaluated by the relations:

$$\begin{aligned}
 A^{B_c {}^3A(^1A)} &= -(m_{B_c} - m_A) q^3 A^{(^1A)}, \\
 V_1^{B_c {}^3A(^1A)} &= -l^3 A^{(^1A)} / (m_{B_c} - m_A), \\
 V_2^{B_c {}^3A(^1A)} &= (m_{B_c} - m_A) c_+^3 A^{(^1A)}, \tag{6.16} \\
 V_0^{B_c {}^3A(^1A)} &= \frac{m_{B_c} - m_A}{2m_A} V_1^{B_c {}^3A(^1A)} - \frac{m_{B_c} + m_A}{2m_A} V_2^{B_c {}^3A(^1A)} \\
 &- \frac{q^2}{2m_A} c_-^3 A^{(^1A)},
 \end{aligned}$$

where $q^3 A^{(^1A)}, l^3 A^{(^1A)},$ and $c_\pm^3 A^{(^1A)}$ are functions of q^2 , with the concrete expressions in the CLFQM as [191, 197, 202]

$$\begin{aligned}
 q^3 A^{(^1A)}(q^2) &= -\frac{N_c}{16\pi^3} \int dx_2 d^2 \vec{k}_{2\perp} \frac{2h'_{B_c} h''_{A(^1A)}}{x_2 \hat{N}'_1 \hat{N}''_1} \\
 &\times \left\{ \frac{2}{\omega''_{A(^1A)}} \left[\vec{k}'_\perp{}^2 + \frac{(\vec{k}'_\perp \cdot \vec{q}_\perp)^2}{2^2} \right] \right.
 \end{aligned}$$

$$\times \left(+ x_2 m'_1 + x_1 m_2 + (m'_1 + m''_1) \frac{\vec{k}'_{\perp} \cdot \vec{q}_{\perp}}{q^2} \right) \Big\}, \tag{6.17}$$

$$\begin{aligned} I^{3A^{(1A)}}(q^2) &= \frac{N_c}{16\pi^3} \int dx_2 d^2 \vec{k}'_{\perp} \frac{h'_{B_c} h''_{3A^{(1A)}}}{x_2 \hat{N}'_1 \hat{N}''_1} \\ &\times \left\{ -4 \frac{q^2 \vec{k}'_{\perp}{}^2 + (\vec{k}'_{\perp} \cdot \vec{q}_{\perp})^2}{q^2 \omega''_{3A^{(1A)}}} \right. \\ &\times \left[2x_1 (M'^2 + M_0'^2) - q^2 - P \cdot q - 2(q^2 + P \cdot q) \frac{\vec{k}'_{\perp} \cdot \vec{q}_{\perp}}{q^2} \right. \\ &\left. \left. - 2(m'_1 + m''_1)(m'_1 - m_2) \right] \right. \\ &\times \left(+ 2x_1 (m_2 - m'_1)(M_0^2 + M_0'^2) + 4x_1 m''_1 M_0^2 \right. \\ &+ 2x_2 m'_1 P \cdot q + 2m_2 q^2 - 2x_1 m_2 \\ &\times (M'^2 + M''^2) + 2(m'_1 - m_2)(m'_1 - m''_1)^2 \\ &+ 8(m'_1 - m_2) \left[\vec{k}'_{\perp}{}^2 + \frac{(\vec{k}'_{\perp} \cdot \vec{q}_{\perp})^2}{q^2} \right] \\ &\left. \left. + 2(m'_1 - m''_1)(q^2 + P \cdot q) \frac{\vec{k}'_{\perp} \cdot \vec{q}_{\perp}}{q^2} \right) \right\}, \tag{6.18} \end{aligned}$$

$$\begin{aligned} c_+^{3A^{(1A)}}(q^2) &= \frac{N_c}{16\pi^3} \int dx_2 d^2 \vec{k}'_{\perp} \frac{2h'_{B_c} h''_{3A^{(1A)}}}{x_2 \hat{N}'_1 \hat{N}''_1} \\ &\times \left\{ -2 \frac{x_2 q^2 + \vec{k}'_{\perp} \cdot \vec{q}_{\perp}}{x_2 q^2 \omega''_{3A^{(1A)}}} \right. \\ &\times \left[\vec{k}'_{\perp} \cdot \vec{k}''_{\perp} + (x_1 m_2 + x_2 m'_1)(x_1 m_2 + x_2 m''_1) \right] \\ &\times \left(+ (x_1 - x_2)(x_2 m'_1 + x_1 m_2) - [2x_1 m_2 - m''_1 \right. \\ &\left. + (x_2 - x_1) m'_1] \frac{\vec{k}'_{\perp} \cdot \vec{q}_{\perp}}{q^2} \right) \Big\}, \tag{6.19} \end{aligned}$$

$$\begin{aligned} c_-^{3A^{(1A)}}(q^2) &= \frac{N_c}{16\pi^3} \int dx_2 d^2 \vec{k}'_{\perp} \frac{h'_{B_c} h''_{3A^{(1A)}}}{x_2 \hat{N}'_1 \hat{N}''_1} \\ &\times \left(\frac{4}{\omega''_{3A^{(1A)}}} \left([M^2 + M''^2 - q^2 + 2(m'_1 - m_2)(-m''_1 + m_2)] \right. \right. \\ &(A_3^2 + A_4^{(2)} - A_2^1) + Z_2(3A_2^{(1)} - 2A_4^{(2)} - 1) \\ &+ \frac{1}{2} P \cdot q (A_1^{(1)} + A_2^{(1)} - 1) [x_1 (q^2 + P \cdot q) \\ &- 2M^2 - 2\vec{k}'_{\perp} \cdot \vec{q}_{\perp} - 2m'_1(-m''_1 + m_2 \\ &- 2m_2(m'_1 - m_2))] \left[\frac{\vec{k}'_{\perp}{}^2}{q^2} + \frac{(\vec{k}'_{\perp} \cdot \vec{q}_{\perp})^2}{q^4} \right] (4A_2^{(1)} - 3) \Big) \\ &\times \left(+ 2(2x_1 - 3)(x_2 m'_1 + x_1 m_2) - 8(m'_1 - m_2) \right. \\ &\times \left[\frac{\vec{k}'_{\perp}{}^2}{q^2} + 2 \frac{(\vec{k}'_{\perp} \cdot \vec{q}_{\perp})^2}{q^4} \right] \\ &\left. - [(14 - 12x_1)m'_1 + 2m''_1 - (8 - 12x_1)m_2] \frac{\vec{k}'_{\perp} \cdot \vec{q}_{\perp}}{q^2} \right) \Big\}, \tag{6.20} \end{aligned}$$

where

$$\begin{aligned} h''_{3A} &= (M''^2 - M_0'^2) \sqrt{\frac{x_1 x_2}{N_c}} \frac{1}{\sqrt{2\tilde{M}_0''}} \frac{\tilde{M}_0''}{2\sqrt{2}M_0''} \phi_p(x_2, \vec{k}'_{\perp}), \\ h''_{1A} &= (M''^2 - M_0'^2) \sqrt{\frac{x_1 x_2}{N_c}} \frac{1}{\sqrt{2\tilde{M}_0''}} \phi_p(x_2, \vec{k}'_{\perp}), \tag{6.21} \end{aligned}$$

$$\omega''_{3A} = \frac{\tilde{M}_0'^2}{m''_1 - m_2}, \text{ and } \omega''_{1A} = 2.$$

In the previous theoretical works [191–197], the phenomenological Gaussian-type wave functions

$$\begin{aligned} \phi_s(x_2, \vec{k}'_{\perp}) &= 4 \left(\frac{\pi}{\beta'^{(l)2}} \right)^{3/4} \sqrt{\frac{e_1^{(l)} e_2}{x_1 x_2 M_0'^{(l)}}} \exp \left(- \frac{\vec{k}'_{\perp}{}^2 + k_z'^{(l)2}}{2\beta'^{(l)2}} \right), \\ \phi_p(x_2, \vec{k}'_{\perp}) &= 4 \left(\frac{\pi}{\beta'^2} \right)^{3/4} \sqrt{\frac{2}{\beta'^2}} \sqrt{\frac{e_1' e_2}{x_1 x_2 M_0''}} \exp \left(- \frac{\vec{k}'_{\perp}{}^2 + k_z'^2}{2\beta'^2} \right) \tag{6.22} \end{aligned}$$

with

$$\begin{aligned} k_z'^{(l)} &= \frac{x_2 M_0'^{(l)}}{2} - \frac{m_2^2 + \vec{k}'_{\perp}{}^2}{2x_2 M_0'^{(l)}}, \\ e_1'^{(l)} &= \sqrt{m_1'^{(l)2} + \vec{k}'_{\perp}{}^2 + k_z'^{(l)2}}, \\ e_2 &= \sqrt{m_2^2 + \vec{k}'_{\perp}{}^2 + k_z'^2}, \tag{6.23} \end{aligned}$$

are widely used. However, this treatment unavoidably results in the dependence of decay width on the parameter β , which is a parameter within the utilized SHO wave function. In this study, we capitalize on the knowledge acquired from the discussion on meson spectrum employing the MGI model in Sect. 2 to acquire the numerical spatial wave functions of the mesons under consideration. To accomplish this, we replace the form provided in Eq. (6.22) with a refined expression

$$\begin{aligned} \phi_l(x_2, \vec{k}'_{\perp}) &= \sqrt{4\pi} \sum_{n=1}^{N_{\max}} c_n \sqrt{\frac{e_1^{(l)} e_2}{x_1 x_2 M_0'^{(l)}}} R_{nl} \left(\sqrt{\vec{k}'_{\perp}{}^2 + k_z'^{(l)2}} \right), \\ \phi_s(x_2, \vec{k}'_{\perp}) &\equiv \phi_{l=0}(x_2, \vec{k}'_{\perp}), \\ \phi_p(x_2, \vec{k}'_{\perp}) &\equiv \phi_{l=1}(x_2, \vec{k}'_{\perp}), \tag{6.24} \end{aligned}$$

where the expansion coefficients c_n represent the values of the corresponding eigenvectors, while l denotes the orbital angular momentum of the meson. By incorporating these modifications, we can effectively eliminate the associated uncertainties. To ensure proper normalization, the inclusion of the factor $\sqrt{4\pi}$ is necessary, i.e.,

$$\int \frac{dx_2 d^2 \vec{k}'_{\perp}}{2(2\pi)^3} \phi_l^*(x_2, \vec{k}'_{\perp}) \phi_l(x_2, \vec{k}'_{\perp}) = 1. \tag{6.25}$$

Besides, $R_{nl}(|p|)$ is the SHO wave function as

$$R_{nl}(|p|) = \frac{(-1)^{n-1}}{\beta^{3/2}} \sqrt{\frac{2(n-1)!}{\Gamma(n+l+1/2)}} \left(\frac{p}{\beta} \right)^l$$

$$\times \exp\left(-\frac{p^2}{2\beta^2}\right)L_{n-1}\left(\frac{p^2}{\beta^2}\right). \tag{6.26}$$

The parameter $\beta = 0.5 \text{ GeV}$ used in the above equation is consistent with Sect. 2. In Eq. (6.26), we neglect the factor $(-i)^l$ since it does not affect the final results, but it does introduce a common factor of i to the P -wave final state weak transition form factors, which makes the form factors less concise.

Following the approach described in Refs. [201,202], we adopt the condition $q^+ = 0$. This implies that our form factor calculations are performed in the space-like region ($q^2 < 0$), and therefore we need to extrapolate them to the time-like region ($q^2 > 0$). To perform the analytical continuations, we utilize the z -series parametrization [204], which has the form as [205]¹

$$\mathcal{F}(q^2) = \frac{1}{1 - q^2/m_{\text{pole}}^2} \left[a_0 + a_1 \left(z(q^2) - z(0) - \frac{1}{3}(z(q^2)^2 - z(0)^2) \right) + a_2 \left(z(q^2) - z(0) + \frac{2}{3}(z(q^2)^2 - z(0)^2) \right) \right], \tag{6.27}$$

where a_0, a_1 , and a_2 are free parameters needed to be fitted in $q^2 < 0$ region, and $z(q^2)$ is written as [204,206,207]

$$z(q^2) = \frac{\sqrt{t_+ - q^2} - \sqrt{t_+ - t_0}}{\sqrt{t_+ - q^2} + \sqrt{t_+ - t_0}} \tag{6.28}$$

with $t_0 = t_+ \left(1 - \sqrt{1 - t_-/t_+}\right)$ and $t_{\pm} = (m_{B_c} \pm m_f)^2$. m_{B_c} and m_f are the masses of the B_c meson and daughter meson, respectively. This parametrization are more convenient to reflect the character $F_1^{B_c P(S)}(q^2 = 0) = F_0^{B_c P(S)}(q^2 = 0)$. Moreover, we have $\mathcal{F}(0) = a_0$.

To determine the values of the free parameters a_0, a_1 , and a_2 ,² as stated in Eq. (6.27), we perform numerical calculations at 200 equally spaced points for each form factor, ranging from -20 GeV^2 to -0.1 GeV^2 , utilizing Eqs. (6.3)–(6.20). Subsequently, we fit the calculated points using Eq. (6.27). The fitted values of the free parameters, as well as $\mathcal{F}(0), \mathcal{F}(q_{\text{max}}^2)$, and the pole masses m_{pole} , are compiled in Tables 10 (11, 12, 13) for $B_c \rightarrow P(V, S, A)$ transitions. Additionally, the q^2 dependence of the $B_c \rightarrow P(V, S, A)$ transition form factors is illustrated in Figs. 4 (5, 6, 7). Particularly, in the $B_c \rightarrow \eta_c$ panel, we also present the LQCD’s result [179]. Our result is slightly larger than the LQCD in low q^2 region, but is anastomotic in large q^2 region.

With the obtained weak transition form factors, we can future investigate the corresponding semileptonic decays. For

¹ We employ a uniform representation, denoted as $\mathcal{F}(q^2)$, to encompass all the relevant form factors.

² For $B_c \rightarrow P(S)$ transitions, only the parameters a_1 and a_2 need to be fitted, as a_0 can be obtained from $\mathcal{F}(0)$ using Eq. (6.27), and $\mathcal{F}(0)$ can be accurately calculated using Eqs. (6.3) and (6.7).

the $B_c \rightarrow M\ell\nu_\ell$ processes, the differential decay width can be obtained by

$$\frac{d^2\Gamma}{dq^2 d\cos\theta_\ell} = \frac{G_F^2 V_{\text{CKM}}^2 \sqrt{\lambda(m_{B_c}^2, m_M^2, q^2)}(1 - \hat{m}_\ell^2)}{512\pi^3 2m_{B_c}^3} \times \left(L_1 + L_2 \cos\theta_\ell + L_3 \cos 2\theta_\ell \right), \tag{6.29}$$

where $G_F = 1.16637 \times 10^{-5} \text{ GeV}^{-2}$ is the Fermi coupling constant, V_{CKM} is the Cabibbo–Kobayashi–Maskawa (CKM) matrix element, $\lambda(x, y, z) = x^2 + y^2 + z^2 - 2(xy + xz + yz)$ is the Källén function, m_M is the mass of the daughter meson, and $\hat{m}_\ell^2 = m_\ell^2/q^2$ with m_ℓ being the lepton mass. The angular coefficients $L_{1,2,3}$ for $M = P(S)$ are

$$L_1 = 2(1 - \hat{m}_\ell^2) \left(2F_0^2(m_{B_c}^2 - m_{P(S)}^2)^2 \hat{m}_\ell^2 + F_1^2 \lambda(m_{B_c}^2, m_{P(S)}^2, q^2) (1 + \hat{m}_\ell^2) \right), \tag{6.30}$$

$$L_2 = -8F_0 F_1 \hat{m}_\ell^2 (m_{B_c}^2 - m_{P(S)}^2) (1 - \hat{m}_\ell^2) \sqrt{\lambda(m_{B_c}^2, m_{P(S)}^2, q^2)}, \tag{6.31}$$

$$L_3 = -2F_1^2 (1 - \hat{m}_\ell^2)^2 \lambda(m_{B_c}^2, m_{P(S)}^2, q^2), \tag{6.32}$$

and for $M = V(A)$ are

$$L_1 = (1 - \hat{m}_\ell^2) \left(4A(V)_0^2 \lambda(m_{B_c}^2, m_{V(A)}^2, q^2) \hat{m}_\ell^2 + \frac{1 + \hat{m}_\ell^2}{2m_{V(A)}^2} \times \left[A(V)_1(m_{B_c} \pm m_{V(A)})(m_{B_c}^2 - m_{V(A)}^2 - q^2) - A(V)_2 \frac{\lambda(m_{B_c}^2, m_{V(A)}^2, q^2)}{m_{B_c} \pm m_{V(A)}} \right]^2 \right) + \frac{2(1 - \hat{m}_\ell^2)}{(m_{B_c} \pm m_{V(A)})^2} (3 + \hat{m}_\ell^2) q^2 \left[A(V)_1^2 (m_{B_c} \pm m_{V(A)})^4 + V(A)^2 \lambda(m_{B_c}^2, m_{V(A)}^2, q^2) \right], \tag{6.33}$$

$$L_2 = \frac{4A(V)_0 \hat{m}_\ell^2 (1 - \hat{m}_\ell^2)}{m_{V(A)}(m_{B_c} \pm m_{V(A)})} \sqrt{\lambda(m_{B_c}^2, m_{V(A)}^2, q^2)} \times \left[A(V)_2 \lambda(m_{B_c}^2, m_{V(A)}^2, q^2) - A(V)_1 (m_{B_c} \pm m_{V(A)})^2 (m_{B_c}^2 - m_{V(A)}^2 - q^2) \right] \pm 16A(V)_1 V (1 - \hat{m}_\ell^2) q^2 \sqrt{\lambda(m_{B_c}^2, m_{V(A)}^2, q^2)}, \tag{6.34}$$

$$L_3 = -\frac{(1 - \hat{m}_\ell^2)^2}{2m_{V(A)}^2 (m_{B_c} \pm m_{V(A)})^2} \left[A(V)_1 (m_{B_c} \pm m_{V(A)})^2 \times (m_{B_c}^2 - m_{V(A)}^2 - q^2) - A(V)_2 \lambda(m_{B_c}^2, m_{V(A)}^2, q^2) \right]^2 + \frac{2(1 - \hat{m}_\ell^2) q^2}{(m_{B_c} \pm m_{V(A)})^2} \left[A(V)_1^2 (m_{B_c} \pm m_{V(A)})^4 + V(A)^2 \lambda(m_{B_c}^2, m_{V(A)}^2, q^2) \right]. \tag{6.35}$$

After performing the integral of the angle θ_ℓ , the differential decay width can be obtained by

$$\frac{d\Gamma}{dq^2} = \frac{G_F^2 V_{\text{CKM}}^2 \sqrt{\lambda(m_{B_c}^2, m_M^2, q^2)}(1 - \hat{m}_\ell^2)}{512\pi^3 2m_{B_c}^3} \left(2L_1 - \frac{2}{3}L_3 \right). \tag{6.36}$$

Table 10 The form factors of the $B_c \rightarrow B_s, B, D, \eta_c$ transitions in CLFQM

	$\mathcal{F}(0) = a_0$	$\mathcal{F}(q_{\max}^2)$	$m_{\text{pole}} \text{ (GeV)}$	a_1	a_2
$F_1^{B_c \rightarrow B_s}$	0.703	0.923	2.112	-32.550	515.53
$F_0^{B_c \rightarrow B_s}$	0.703	0.831	2.460	-9.520	-13.871
$F_1^{B_c \rightarrow B}$	0.615	0.886	2.007	-28.916	447.924
$F_0^{B_c \rightarrow B}$	0.615	0.757	2.412	-7.279	-69.149
$F_1^{B_c \rightarrow D}$	0.309	1.446	5.325	-1.682	2.017
$F_0^{B_c \rightarrow D}$	0.309	0.605	5.675	0.802	-3.070
$F_1^{B_c \rightarrow \eta_c}$	0.650	1.103	6.336	-4.612	12.277
$F_0^{B_c \rightarrow \eta_c}$	0.650	0.891	6.706	-0.777	1.108

Table 11 The form factors of the $B_c \rightarrow B_s^*, B^*, D^*, J/\psi, \psi(2S)$ transitions in CLFQM

	$\mathcal{F}(0) = a_0$	$\mathcal{F}(q_{\max}^2)$	m_{pole}	a_1	a_2
$V^{B_c \rightarrow B_s^*}$	2.921	3.767	2.112	-164.601	2805.64
$A_0^{B_c \rightarrow B_s^*}$	0.447	0.601	1.968	-29.193	615.132
$A_1^{B_c \rightarrow B_s^*}$	0.425	0.507	2.535	-17.847	278.218
$A_2^{B_c \rightarrow B_s^*}$	0.158	0.168	2.535	7.108	-254.943
$V^{B_c \rightarrow B^*}$	2.672	3.780	2.007	-156.204	2657.84
$A_0^{B_c \rightarrow B^*}$	0.353	0.534	1.865	-25.298	550.667
$A_1^{B_c \rightarrow B^*}$	0.328	0.413	2.422	-12.978	188.302
$A_2^{B_c \rightarrow B^*}$	0.012	-0.022	2.422	18.505	-479.418
$V^{B_c \rightarrow D^*}$	0.326	1.592	5.325	-3.167	7.189
$A_0^{B_c \rightarrow D^*}$	0.281	0.585	5.280	0.944	71.415
$A_1^{B_c \rightarrow D^*}$	0.198	0.499	5.726	-0.312	-0.704
$A_2^{B_c \rightarrow D^*}$	0.119	0.373	5.726	-0.615	0.440
$V^{B_c \rightarrow J/\psi}$	0.804	1.395	6.336	-7.864	26.235
$A_0^{B_c \rightarrow J/\psi}$	0.681	0.987	6.274	-1.761	72.843
$A_1^{B_c \rightarrow J/\psi}$	0.597	0.867	6.749	-2.543	5.721
$A_2^{B_c \rightarrow J/\psi}$	0.434	0.714	6.749	-3.994	13.044
$V^{B_c \rightarrow \psi(2S)}$	0.429	0.407	6.336	5.159	-67.300
$A_0^{B_c \rightarrow \psi(2S)}$	0.357	0.306	6.274	5.929	-23.284
$A_1^{B_c \rightarrow \psi(2S)}$	0.276	0.206	6.749	5.704	-46.34
$A_2^{B_c \rightarrow \psi(2S)}$	0.047	-0.086	6.749	6.922	-61.037

Table 12 The form factors of the $B_c \rightarrow B_{s0}, B_0, D_0^*, \chi_{c0}$ transitions in CLFQM

	$\mathcal{F}(0) = a_0$	$\mathcal{F}(q_{\max}^2)$	m_{pole}	a_1	a_2
$F_1^{B_c \rightarrow B_{s0}}$	0.428	0.449	2.535	-11.305	126.279
$F_0^{B_c \rightarrow B_{s0}}$	0.428	0.381	1.968	179.073	-3346.19
$F_1^{B_c \rightarrow B_0}$	0.468	0.501	2.422	-4.449	-65.925
$F_0^{B_c \rightarrow B_0}$	0.468	0.398	1.865	175.706	-2991.27
$F_1^{B_c \rightarrow D_0}$	0.355	0.782	5.726	0.007	-3.225
$F_0^{B_c \rightarrow D_0}$	0.355	0.126	5.280	4.130	-2.009
$F_1^{B_c \rightarrow \chi_{c0}}$	0.337	0.462	6.749	-1.861	4.133
$F_0^{B_c \rightarrow \chi_{c0}}$	0.337	0.184	6.274	8.389	-23.161

Table 13 The form factors of the $B_c \rightarrow B_{s1}^{(\prime)}, B_1^{(\prime)}, D_1^{(\prime)}, h_c, \chi_{c1}$ transitions in CLFQM

	$\mathcal{F}(0) = a_0$	$\mathcal{F}(q_{\max}^2)$	m_{pole}	a_1	a_2
$A^{B_c \rightarrow B'_{s1}}$	-0.038	-0.039	2.535	1.605	-24.722
$V_0^{B_c \rightarrow B'_{s1}}$	0.232	0.235	2.460	11.187	239.345
$V_1^{B_c \rightarrow B'_{s1}}$	3.444	3.682	2.112	-357.075	6870.02
$V_2^{B_c \rightarrow B'_{s1}}$	-0.087	-0.092	2.112	5.528	-107.399
$A^{B_c \rightarrow B_{s1}}$	0.074	0.077	2.535	-3.468	57.551
$V_0^{B_c \rightarrow B_{s1}}$	0.166	0.176	2.460	-14.452	378.227
$V_1^{B_c \rightarrow B_{s1}}$	3.904	4.010	2.112	199.722	-5484.34
$V_2^{B_c \rightarrow B_{s1}}$	-0.039	-0.042	2.112	3.266	-66.969
$A^{B_c \rightarrow B'_1}$	-0.050	-0.052	2.422	1.640	-19.246
$V_0^{B_c \rightarrow B'_1}$	0.177	0.178	2.412	15.181	150.109
$V_1^{B_c \rightarrow B'_1}$	1.667	1.890	2.007	-351.092	7009.86
$V_2^{B_c \rightarrow B'_1}$	-0.085	-0.091	2.007	5.153	-98.674
$A^{B_c \rightarrow B_1}$	0.085	0.093	2.422	-3.474	50.953
$V_0^{B_c \rightarrow B_1}$	0.208	0.230	2.412	-14.503	390.001
$V_1^{B_c \rightarrow B_1}$	3.205	3.419	2.007	127.525	-3507.11
$V_2^{B_c \rightarrow B_1}$	-0.054	-0.062	2.007	4.546	-91.094
$A^{B_c \rightarrow D'_1}$	0.144	0.328	5.726	-0.662	0.696
$V_0^{B_c \rightarrow D'_1}$	0.258	-0.025	5.675	4.944	85.952
$V_1^{B_c \rightarrow D'_1}$	0.334	0.401	5.325	2.608	-6.499
$V_2^{B_c \rightarrow D'_1}$	0.003	-0.076	5.325	0.732	-3.113
$A^{B_c \rightarrow D_1}$	0.118	0.250	5.726	-0.329	-0.344
$V_0^{B_c \rightarrow D_1}$	-0.147	0.988	5.675	-12.231	-152.47
$V_1^{B_c \rightarrow D_1}$	0.176	-0.0004	5.325	3.202	-6.365
$V_2^{B_c \rightarrow D_1}$	0.160	0.463	5.325	-1.074	2.322
$A^{B_c \rightarrow \chi_{c1}}$	0.215	0.303	6.749	-1.771	5.620
$V_0^{B_c \rightarrow \chi_{c1}}$	0.025	0.066	6.706	-1.462	5.819
$V_1^{B_c \rightarrow \chi_{c1}}$	0.339	0.129	6.336	11.333	-47.961
$V_2^{B_c \rightarrow \chi_{c1}}$	0.078	0.097	6.336	-0.044	-1.797
$A^{B_c \rightarrow h_c}$	0.039	0.056	6.749	-0.372	1.332
$V_0^{B_c \rightarrow h_c}$	0.390	0.110	6.706	14.548	181.296
$V_1^{B_c \rightarrow h_c}$	0.298	0.372	6.336	-0.185	-2.383
$V_2^{B_c \rightarrow h_c}$	-0.196	-0.312	6.336	2.783	-12.591

And then, the decay width can be obtained by carrying out the integral of q^2 in the range of m_ℓ^2 to q_{\max}^2 .

In addition, the differential branching decay widths from the longitudinal and transverse polarizations for $B_c \rightarrow V(A)\ell\nu_\ell$ are

$$\frac{d\Gamma_L}{dq^2} = \frac{G_F^2 V_{CKM}^2}{192\pi^3 m_{B_c}^3} \frac{\sqrt{\lambda(m_{B_c}^2, m_{V(A)}^2, q^2)}}{2} (1 - \hat{m}_\ell^2)^2 \times \left\{ 3\hat{m}_\ell^2 \lambda(m_{B_c}^2, m_{V(A)}^2, q^2) A(V)_0^2 + \frac{2 + \hat{m}_\ell^2}{4m_{V(A)}^2} \right.$$

$$\times \left[A(V)_1(m_{B_c} \pm m_{V(A)})(m_{B_c}^2 - m_{V(A)}^2 - q^2) - A(V)_2 \frac{\lambda(m_{B_c}^2, m_{V(A)}^2, q^2)}{m_{B_c} \pm m_{V(A)}} \right]^2 \Big\}, \tag{6.37}$$

$$\frac{d\Gamma_T}{dq^2} = \frac{G_F^2 V_{CKM}^2}{192\pi^3 m_{B_c}^3} \lambda^{3/2}(m_{B_c}^2, m_{V(A)}^2, q^2) (1 - \hat{m}_\ell^2)^2 (2 + \hat{m}_\ell^2) q^2 \times \left[\frac{A(V)_1^2(m_{B_c} \pm m_{V(A)})^2}{\lambda(m_{B_c}^2, m_{V(A)}^2, q^2)} + \frac{V(A)^2}{(m_{B_c} \pm m_{V(A)})^2} \right]. \tag{6.38}$$

Using the obtained form factors as inputs, we further calculate the corresponding branching ratios and the Γ_L/Γ_T

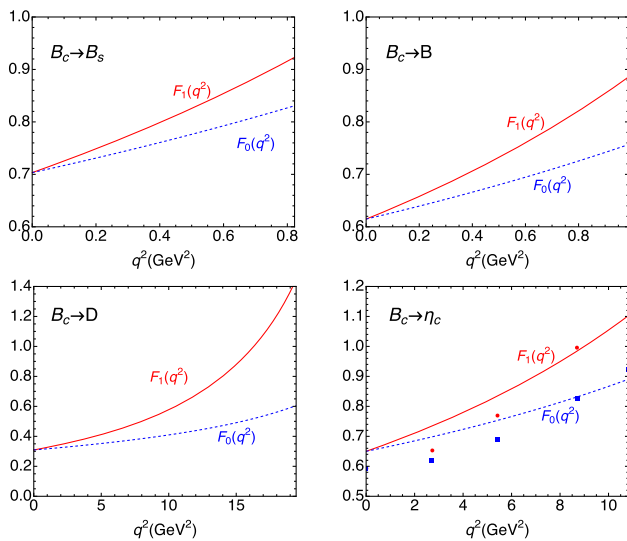


Fig. 4 The q^2 dependence of the weak transition form factors of the $B_c \rightarrow B_s, B, D, \eta_c$ processes. In the $B_c \rightarrow \eta_c$ transition, the form factors F_1 and F_0 are also depicted as the results from LQCD, represented by a red circle and a blue square, respectively, as shown in Figure of Ref. [179]

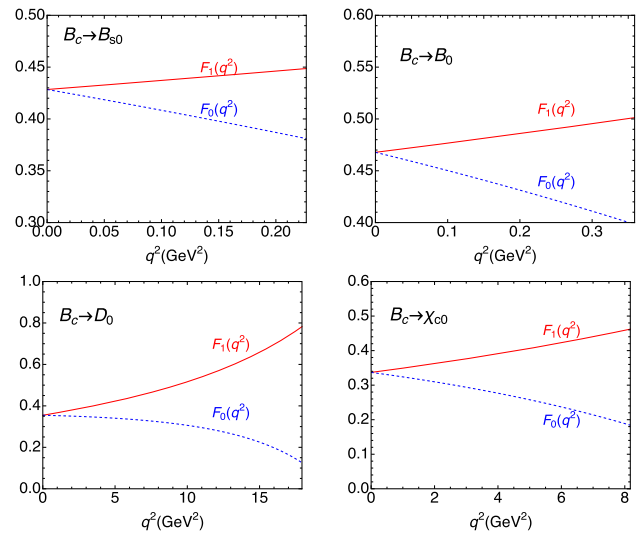


Fig. 6 The q^2 dependence of the weak transition form factors of the $B_c \rightarrow B_{s0}, B_0, D_0, \chi_{c0}$ processes

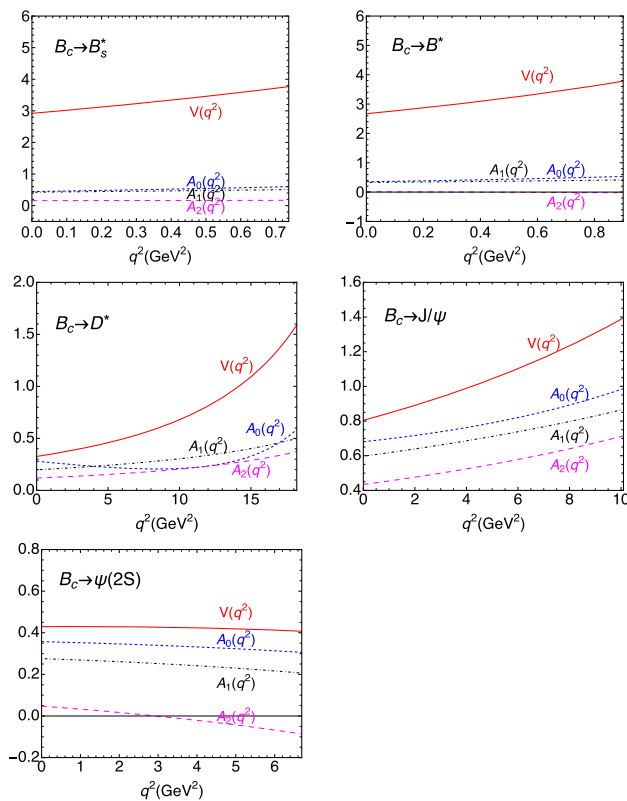


Fig. 5 The q^2 dependence of the weak transition form factors of the $B_c \rightarrow B_s^*, B^*, D^*, J/\psi, \psi(2S)$ processes

ratios. The obtained results are presented in Tables 14, 15, 16, and 17. Additionally, we also compare our obtained branching ratios with those obtained from other theoretical works [192, 193, 195] in the respective tables, and our obtained results are consistent with those from other theoretical works. The branching ratios of the processes $B_c \rightarrow B_s^{(*)} \ell \nu_\ell$ and $B_c \rightarrow J/\psi(\eta_c) \ell \nu_\ell$ can reach up to the order of magnitude of 10^{-2} . The measurements of the absolute branching ratios could be reachable at the ongoing LHCb experiment.

Of particular interest is our result for the ratio

$$\frac{\mathcal{B}(B_c \rightarrow J/\psi \tau \nu_\tau)}{\mathcal{B}(B_c \rightarrow J/\psi \mu \nu_\mu)} = 0.231,$$

which is noticeably smaller than the central value of the experimental measurement $0.71 \pm 0.17 \pm 0.18$ reported by the LHCb Collaboration [208], but is consistent with those from Refs. [192, 198]. This ratio can be used to test the lepton flavor universality, and the misfit of the theoretical and experimental values maybe indicates the new physics effects beyond the Standard Model. A more precise experiment and more theoretical calculations would greatly aid in testing the lepton flavor universality.

Moreover, utilizing the obtained form factors, we can make predictions for nonleptonic decays. Specifically, we explore the processes $B_c \rightarrow J/\psi \pi(K)$, $B_c \rightarrow \psi(2S)\pi$, and $B_c \rightarrow \chi_{c0}\pi$, since they have corresponding experimental measurements. Assuming the naive factorization assumption, the branching ratios for these decays can be calculated as described in [197]

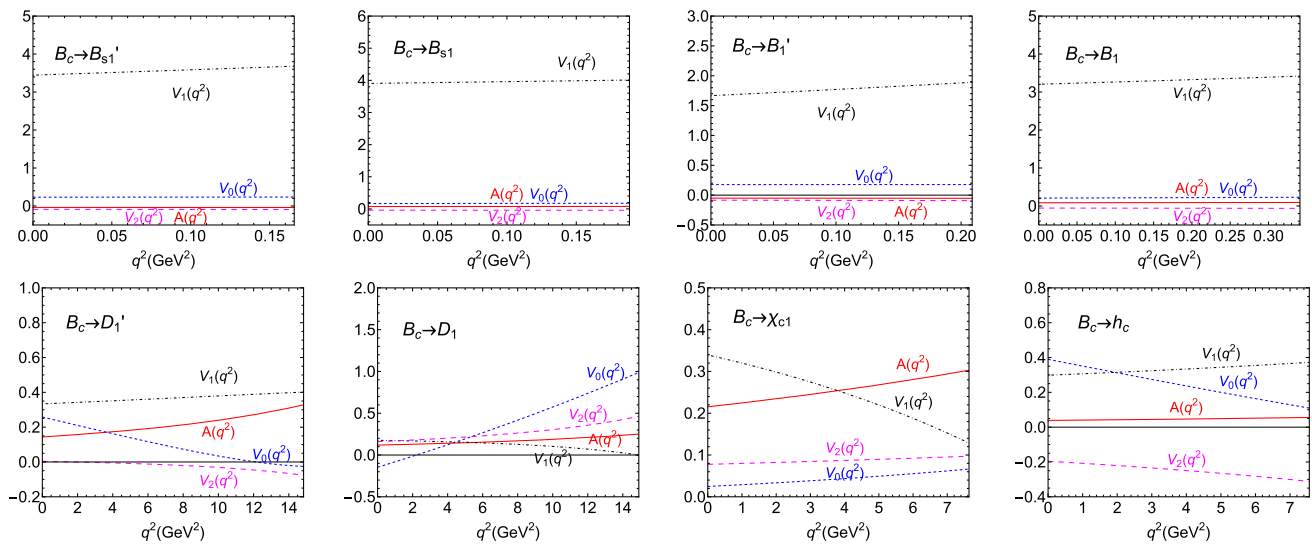


Fig. 7 The q^2 dependence of the weak transition form factors of the $B_c \rightarrow B_{s1}^{(\prime)}, B_1^{(\prime)}, D_1^{(\prime)}, \chi_{c1}, h_c$ processes

$$\begin{aligned}
 & \mathcal{B}(B_c \rightarrow J/\psi(\psi(2S))\pi(K)) \\
 &= \frac{\left| G_F V_{cb} V_{ud(us)} a_1 f_{\pi(K)} m_{B_c}^2 A_0^{B_c J/\psi(\psi(2S))} (m_{\pi(K)}^2) \right|^2}{32\pi m_{B_c} \Gamma_{B_c}} \\
 & \times \left(1 - \frac{m_{J/\psi(\psi(2S))}^2}{m_{B_c}^2} \right), \tag{6.39}
 \end{aligned}$$

$$\begin{aligned}
 & \mathcal{B}(B_c \rightarrow \chi_{c0}\pi) \\
 &= \frac{\left| G_F V_{cb} V_{ud} a_1 f_{\pi} m_{B_c}^2 F_0^{B_c \chi_{c0}} (m_{\pi}^2) \right|^2}{32\pi m_{B_c} \Gamma_{B_c}} \left(1 - \frac{m_{\chi_{c0}}^2}{m_{B_c}^2} \right),
 \end{aligned}$$

where $a_1 = 1.07$ and $a_2 = 0.234$ [197].

The concerned branching ratios are determined as

$$\begin{aligned}
 \mathcal{B}(B_c \rightarrow J/\psi\pi) &= 2.785 \times 10^{-3}, \\
 \mathcal{B}(B_c \rightarrow J/\psi K) &= 0.213 \times 10^{-3}, \\
 \mathcal{B}(B_c \rightarrow \psi(2S)\pi) &= 0.662 \times 10^{-3},
 \end{aligned}$$

and some ratios of the branching ratios are

$$\begin{aligned}
 R_{J/\psi}^{K/\pi} &= \frac{\mathcal{B}(B_c \rightarrow J/\psi K)}{\mathcal{B}(B_c \rightarrow J/\psi \pi)} = 0.077, \\
 R_{\pi}^{\psi(2S)/J/\psi} &= \frac{\mathcal{B}(B_c \rightarrow \psi(2S)\pi)}{\mathcal{B}(B_c \rightarrow J/\psi \pi)} = 0.238, \\
 R_{J/\psi}^{\pi/\mu\nu\mu} &= \frac{\mathcal{B}(B_c \rightarrow J/\psi \pi)}{\mathcal{B}(B_c \rightarrow J/\psi \mu\nu\mu)} = 0.131.
 \end{aligned}$$

Two of these predictions are in agreement with the experimental values: $R_{J/\psi}^{K/\pi} = 0.079 \pm 0.007 \pm 0.003$ and $R_{\pi}^{\psi(2S)/J/\psi} = 0.268 \pm 0.032 \pm 0.007 \pm 0.006$ [46]. However, the prediction for $R_{J/\psi}^{\pi/\mu\nu\mu}$ is apparently larger than the experimental value of $(4.69 \pm 0.28 \pm 0.46) \times 10^{-2}$ [46]. Additionally, we obtain $\mathcal{B}(B_c \rightarrow \chi_{c0}\pi) = 0.633 \times 10^{-3}$,

which is significantly larger than the experimental measurement $(2.4_{-0.8}^{+0.9}) \times 10^{-5}$ reported by the LHCb Collaboration [209], but is consistent with the Ref. [197]. Further experimental measurements are eagerly awaited to provide additional scrutiny and validation of our theoretical predictions for these weak decays.

If the discussed hadron has the near-threshold behaviour, the state should be a mixture of $\bar{b}c$ components and two meson components. The meson components should be important because the coupling is given by a strong mechanism, which gives the important decay widths, and they are enhanced by the denominators of the difference between the energy and the threshold energy position. Thus, the decays through the two meson components will be small and the results given in our work can be seen as an upper limit in most cases.

7 Summary

Although significant progress has been made in observing new hadronic states over the past two decades, the establishment of the B_c meson family remains incomplete, with only B_c^+ and $B_c(2S)^\pm$ states listed in the PDG [46]. With the upgrade being complete of the LHCb experiment in preparation for Run 3 and Run 4 of LHC, we have reason to believe this situation will be changed. Hence, the current work is timely and can provide valuable information for the experimental explorations of B_c mesons.

According to the previous experience of the studies of hadron spectroscopy [60,62,63,65–71,210,211], the importance of the unquenched effects has been realized step by step. The low mass puzzles involved in the $X(3872)$, $D_{s0}(2317)$,

Table 14 The branching ratios of the $B_c \rightarrow B_s(B, D, \eta_c)\ell\nu_\ell$ decays. Additionally, we compare our findings with the branching ratios reported in other theoretical studies

Channels	ℓ	Branching ratios	Ref. [195]	Ref. [192]
$B_c \rightarrow B_s\ell\nu_\ell$	e	1.537×10^{-2}	1.51×10^{-2}	$1.49^{+0.29}_{-0.30} \times 10^{-2}$
	μ	1.452×10^{-2}	1.43×10^{-2}	$1.41^{+0.27}_{-0.28} \times 10^{-2}$
$B_c \rightarrow B\ell\nu_\ell$	e	0.989×10^{-3}	1.04×10^{-3}	$1.09^{+0.26}_{-0.26} \times 10^{-3}$
	μ	0.944×10^{-3}	1.00×10^{-3}	$1.04^{+0.24}_{-0.25} \times 10^{-3}$
$B_c \rightarrow D\ell\nu_\ell$	e	7.024×10^{-5}	...	$3.0^{+1.0}_{-0.9} \times 10^{-5}$
	μ	7.012×10^{-5}	...	$3.0^{+1.0}_{-0.9} \times 10^{-5}$
	τ	3.924×10^{-5}	...	$2.1^{+0.7}_{-0.7} \times 10^{-5}$
$B_c \rightarrow \eta_c\ell\nu_\ell$	e	7.899×10^{-3}	...	$6.7^{+1.1}_{-1.3} \times 10^{-3}$
	μ	7.868×10^{-3}	...	$6.7^{+1.1}_{-1.3} \times 10^{-3}$
	τ	2.187×10^{-3}	...	$1.90^{+0.33}_{-0.34} \times 10^{-3}$

Table 15 The branching ratios and the Γ_L/Γ_T of the $B_c \rightarrow B_s^*(B^*, D^*, J/\psi, \psi(2S))\ell\nu_\ell$ decays. Additionally, we compare our findings with the branching ratios reported in other theoretical studies

Channels	ℓ	Branching ratios	Γ_L/Γ_T	Ref. [192]
$B_c \rightarrow B_s^*\ell\nu_\ell$	e	1.416×10^{-2}	1.123	$1.96^{+0.45}_{-0.44} \times 10^{-2}$
	μ	1.324×10^{-2}	1.099	$1.83^{+0.43}_{-0.41} \times 10^{-2}$
$B_c \rightarrow B^*\ell\nu_\ell$	e	0.777×10^{-3}	1.066	$1.41^{+0.36}_{-0.34} \times 10^{-3}$
	μ	0.736×10^{-3}	1.049	$1.34^{+0.43}_{-0.32} \times 10^{-3}$
$B_c \rightarrow D^*\ell\nu_\ell$	e	1.256×10^{-4}	1.033	$0.45^{+0.16}_{-0.13} \times 10^{-4}$
	μ	1.253×10^{-4}	1.031	$0.45^{+0.16}_{-0.13} \times 10^{-4}$
	τ	0.601×10^{-4}	0.773	$0.27^{+0.10}_{-0.08} \times 10^{-4}$
$B_c \rightarrow J/\psi\ell\nu_\ell$	e	2.130×10^{-2}	1.189	$1.49^{+0.27}_{-0.27} \times 10^{-2}$
	μ	2.119×10^{-2}	1.186	$1.49^{+0.27}_{-0.27} \times 10^{-2}$
	τ	0.489×10^{-2}	0.838	$0.37^{+0.07}_{-0.07} \times 10^{-2}$
$B_c \rightarrow \psi(2S)\ell\nu_\ell$	e	1.311×10^{-3}	1.856	...
	μ	1.298×10^{-3}	1.847	...
	τ	0.071×10^{-3}	0.924	...

Table 16 The branching ratios of the $B_c \rightarrow B_{s0}(B_0, D_0, \chi_{c0})\ell\nu_\ell$ decays. Additionally, we compare our findings with the branching ratios reported in other theoretical studies

Channels	ℓ	Branching ratios	Ref. [193]	Ref. [195]
$B_c \rightarrow B_{s0}\ell\nu_\ell$	e	2.203×10^{-4}	...	6.58×10^{-4}
	μ	1.703×10^{-4}	...	5.23×10^{-4}
$B_c \rightarrow B_0\ell\nu_\ell$	e	0.419×10^{-4}	...	4.60×10^{-5}
	μ	0.354×10^{-4}	...	3.77×10^{-5}
$B_c \rightarrow D_0\ell\nu_\ell$	e	0.547×10^{-4}
	μ	0.545×10^{-4}
	τ	0.202×10^{-4}
$B_c \rightarrow \chi_{c0}\ell\nu_\ell$	e	1.084×10^{-3}	$2.1^{+0.4}_{-0.5} \times 10^{-3}$...
	μ	1.075×10^{-3}	$2.1^{+0.4}_{-0.5} \times 10^{-3}$...
	τ	0.094×10^{-3}	$0.24^{+0.04}_{-0.05} \times 10^{-3}$...

Table 17 The branching ratios and the Γ_L/Γ_T of the $B_c \rightarrow B_{s1}^{(j)}(B_1^{(j)}, D_1^{(j)}, h_c, \chi_{c1})\ell\nu\ell$ decays. Additionally, we compare our findings with the branching ratios reported in other theoretical studies

Channels	ℓ	Branching ratios	Γ_L/Γ_T	Ref. [193]	Ref. [195]
$B_c \rightarrow B_{s1}'\ell\nu\ell$	e	3.946×10^{-5}	2.615	...	5.38×10^{-4}
	μ	2.793×10^{-5}	2.314	...	3.98×10^{-4}
$B_c \rightarrow B_{s1}\ell\nu\ell$	e	5.824×10^{-5}	1.591	...	8.31×10^{-5}
	μ	4.230×10^{-5}	1.379	...	6.33×10^{-5}
$B_c \rightarrow B_1'\ell\nu\ell$	e	1.636×10^{-6}	3.357	...	7.70×10^{-5}
	μ	1.244×10^{-6}	3.097	...	6.28×10^{-5}
$B_c \rightarrow B_1\ell\nu\ell$	e	1.743×10^{-5}	1.708	...	1.52×10^{-5}
	μ	1.461×10^{-5}	1.575	...	1.28×10^{-5}
$B_c \rightarrow D_1'\ell\nu\ell$	e	3.510×10^{-5}	1.736
	μ	3.491×10^{-5}	1.730
	τ	1.026×10^{-5}	0.995
$B_c \rightarrow D_1\ell\nu\ell$	e	0.984×10^{-5}	1.533
	μ	0.979×10^{-5}	1.529
	τ	0.519×10^{-5}	2.940
$B_c \rightarrow h_c\ell\nu\ell$	e	1.155×10^{-3}	11.769	$3.1_{-0.9}^{+0.7} \times 10^{-3}$...
	μ	1.140×10^{-3}	11.669	$3.1_{-0.9}^{+0.7} \times 10^{-3}$...
	τ	0.051×10^{-3}	2.877	$0.22_{-0.05}^{+0.04} \times 10^{-3}$...
$B_c \rightarrow \chi_{c1}\ell\nu\ell$	e	2.953×10^{-4}	0.031	$1.40_{-0.24}^{+0.22} \times 10^{-3}$...
	μ	2.933×10^{-4}	0.031	$1.40_{-0.24}^{+0.22} \times 10^{-3}$...
	τ	0.256×10^{-4}	0.050	$0.15_{-0.03}^{+0.02} \times 10^{-3}$...

$D_{s1}(2460)$, and $\Lambda_c(2940)$ can be well understood under this scenario. In this work, we provide a complete spectroscopy of the B_c mesons under the unquenched picture. We first present the mass spectrum of the B_c mesons, where the MGI model was applied to the concrete calculations, which can reflect the unquenched effects. The obtained mass spectrum of the B_c mesons is valuable, but not sufficient for further experimental search for them. Therefore, in this work, we have investigated their various decay behaviors, including the two-body OZI-allowed strong decays, the dipion transitions between B_c mesons, the radiative decays, and some typical weak decays of $B_c(1^3S_0)$. We must emphasize that the discussed decays of B_c mesons are supported by the mass spectrum study, since we simultaneously obtain the information of the numerical spatial wave functions of these focused B_c mesons associated with their masses, which are used as inputs for the calculations of the B_c meson decays. This treatment avoids the parameter dependence in the decay studies.

With the accumulation of experimental data and enhancement of experimental capabilities, the investigations of hadron spectroscopy will enter a new stage. As an important part of the hadron family, the B_c mesons become focal point, as our knowledge of the B_c meson family is still insufficient. Facing this situation, we have reason to believe that it is full of challenges and opportunities. We expect that our experimental colleagues to seize this opportunity to continue to expand the realm of the observed hadrons.

Acknowledgements This work is supported by the China National Funds for Distinguished Young Scientists under Grant No. 11825503, the National Key Research and Development Program of China under Contract No. 2020YFA0406400, the 111 Project under Grant No. B20063, the National Natural Science Foundation of China under Grant Nos. 12247101 and 12247155, the fundamental Research Funds for the Central Universities, and the project for top-notch innovative talents of Gansu province. F.L.W. is also supported by the China Postdoctoral Science Foundation under Grant No. 2022M721440.

Data availability This manuscript has no associated data or the data will not be deposited. [Authors' comment: This is a theoretical study and no external data are associated with this work.]

Open Access This article is licensed under a Creative Commons Attribution 4.0 International License, which permits use, sharing, adaptation, distribution and reproduction in any medium or format, as long as you give appropriate credit to the original author(s) and the source, provide a link to the Creative Commons licence, and indicate if changes were made. The images or other third party material in this article are included in the article's Creative Commons licence, unless indicated otherwise in a credit line to the material. If material is not included in the article's Creative Commons licence and your intended use is not permitted by statutory regulation or exceeds the permitted use, you will need to obtain permission directly from the copyright holder. To view a copy of this licence, visit <http://creativecommons.org/licenses/by/4.0/>.

Funded by SCOAP³. SCOAP³ supports the goals of the International Year of Basic Sciences for Sustainable Development.

References

1. S. Godfrey, S.L. Olsen, The exotic XYZ charmonium-like mesons. *Ann. Rev. Nucl. Part. Sci.* **58**, 51–73 (2008)
2. B.Q. Li, K.T. Chao, Higher charmonia and X , Y , Z states with screened potential. *Phys. Rev. D* **79**, 094004 (2009)
3. X. Liu, An overview of XYZ new particles. *Chin. Sci. Bull.* **59**, 3815 (2014)
4. C.Z. Yuan [BESIII], Study of the XYZ states at the BESIII. *Front. Phys. (Beijing)* **10**, 101401 (2015)
5. W. Chen, W.Z. Deng, J. He, N. Li, X. Liu, Z.G. Luo, Z.F. Sun, S.L. Zhu, XYZ states. *PoS Hadron* **2013**, 005 (2013)
6. A.N. Hiller Blin, C. Fernández-Ramírez, A. Jackura, V. Mathieu, V.I. Moiseev, A. Pilloni, A.P. Szczepaniak, Studying the $P_c(4450)$ resonance in J/ψ photoproduction off protons. *Phys. Rev. D* **94**, 034002 (2016)
7. F.K. Guo, U.G. Meißner, W. Wang, Z. Yang, How to reveal the exotic nature of the $P_c(4450)$. *Phys. Rev. D* **92**, 071502 (2015)
8. H.X. Chen, W. Chen, X. Liu, S.L. Zhu, The hidden-charm pentaquark and tetraquark states. *Phys. Rep.* **639**, 1 (2016)
9. F.K. Guo, C. Hanhart, U.G. Meißner, Q. Wang, Q. Zhao, B.S. Zou, Hadronic molecules. *Rev. Mod. Phys.* **90**, 015004 (2018)
10. Y.R. Liu, H.X. Chen, W. Chen, X. Liu, S.L. Zhu, Pentaquark and tetraquark states. *Prog. Part. Nucl. Phys.* **107**, 237 (2019)
11. N. Brambilla, S. Eidelman, C. Hanhart, A. Nefediev, C.P. Shen, C.E. Thomas, A. Vairo, C.Z. Yuan, The XYZ states: experimental and theoretical status and perspectives. *Phys. Rep.* **873**, 1 (2020)
12. L. Meng, B. Wang, G.J. Wang, S.L. Zhu, Chiral perturbation theory for heavy hadrons and chiral effective field theory for heavy hadronic molecules. *Phys. Rep.* **1019**, 1–149 (2023)
13. H.X. Chen, W. Chen, X. Liu, Y.R. Liu, S.L. Zhu, An updated review of the new hadron states. *Rep. Prog. Phys.* **86**(2), 026201 (2023)
14. R. Aaij et al. [LHCb], Observation of a narrow pentaquark state, $P_c(4312)^+$, and of two-peak structure of the $P_c(4450)^+$. *Phys. Rev. Lett.* **122**, 222001 (2019)
15. X. Chu [BESIII], Hadron spectroscopy at BESIII. *PoS HQL2016*, 028 (2017)
16. R. Aaij et al. [LHCb], First observation of a doubly charged tetraquark and its neutral partner. *Phys. Rev. Lett.* **131**, 041902 (2023)
17. R. Aaij et al. [LHCb], Amplitude analysis of $B^0 \rightarrow D^0 D_s^+ \pi^-$ and $B^+ \rightarrow D^- D_s^+ \pi^+$ decays. *Phys. Rev. D* **108**, 012017 (2023)
18. J. Wang [LHCb], Heavy flavor and exotic production at LHCb. *PoS ICHEP2022*, 487 (2022)
19. J. Xu [LHCb], LHCb results in charm baryons. *Nucl. Part. Phys. Proc.* **318–323**, 56–60 (2022)
20. Y. Onuki [Belle II], Belle II status and prospect. *Nucl. Part. Phys. Proc.* **318–323**, 78–84 (2022)
21. F. Abudinén et al. [Belle II], Reconstruction of $B \rightarrow \rho \ell \nu_\ell$ decays identified using hadronic decays of the recoil B meson in 2019–2021 Belle II data. [arXiv:2211.15270](https://arxiv.org/abs/2211.15270)
22. K.N. Chu et al. [Belle], Study of $B^+ \rightarrow p \bar{n} \pi^0$. [arXiv:2211.11251](https://arxiv.org/abs/2211.11251)
23. C.H. Chang, Y.Q. Chen, The production of B_c or \bar{B}_c meson associated with two heavy quark jets in Z^0 boson decay. *Phys. Rev. D* **46**, 3845 (1992)
24. C.H. Chang, Y.Q. Chen, The hadronic production of the B_c meson at Tevatron, CERN LHC and SSC. *Phys. Rev. D* **48**, 4086–4091 (1993)
25. F. Abe et al. [CDF], Observation of the B_c meson in $p\bar{p}$ collisions at $\sqrt{s} = 1.8$ TeV. *Phys. Rev. Lett.* **81**, 2432–2437 (1998)
26. M. Lusignoli, M. Masetti, S. Petrarca, B_c production. *Phys. Lett. B* **266**, 142–146 (1991)
27. E. Braaten, K. Cheung, T.C. Yuan, Perturbative QCD fragmentation functions for B_c and B_c^* production. *Phys. Rev. D* **48**, R5049 (1993)
28. C.H. Chang, Y.Q. Chen, R.J. Oakes, Comparative study of the hadronic production of B_c mesons. *Phys. Rev. D* **54**, 4344–4348 (1996)
29. M. Masetti, F. Sartogo, Perturbative predictions for B_c meson production in hadronic collisions. *Phys. Lett. B* **357**, 659–665 (1995)
30. P. Abreu et al. [DELPHI], Search for the B_c meson. *Phys. Lett. B* **398**, 207–222 (1997)
31. K. Ackerstaff et al. [OPAL], Search for the B_c meson in hadronic Z^0 decays. *Phys. Lett. B* **420**, 157–168 (1998)
32. R. Barate et al. [ALEPH], Search for the B_c meson in hadronic Z decays. *Phys. Lett. B* **402**, 213–226 (1997)
33. F. Abe et al. [CDF], Measurement of the branching ratio $B(B_u^+ \rightarrow J/\psi \pi^+)$ and search for $B_c^+ \rightarrow J/\psi \pi^+$. *Phys. Rev. Lett.* **77**, 5176–5181 (1996)
34. A. Abulencia et al. [CDF], Evidence for the exclusive decay $B_c^\pm \rightarrow J/\psi \pi^\pm$ and measurement of the mass of the B_c meson. *Phys. Rev. Lett.* **96**, 082002 (2006)
35. T. Aaltonen et al. [CDF], Observation of the decay $B_c^+ \rightarrow J/\psi \pi^+$ and measurement of the B_c^+ mass. *Phys. Rev. Lett.* **100**, 182002 (2008)
36. V.M. Abazov et al. [D0], Observation of the B_c Meson in the Exclusive Decay $B_c \rightarrow J/\psi \pi$. *Phys. Rev. Lett.* **101**, 012001 (2008)
37. R. Aaij et al. [LHCb], First observation of the decay $B_c^+ \rightarrow J/\psi \pi^+ \pi^- \pi^+$. *Phys. Rev. Lett.* **108**, 251802 (2012)
38. R. Aaij et al. [LHCb], Observation of the decay $B_c^+ \rightarrow \psi(2S) \pi^+$. *Phys. Rev. D* **87**, 071103 (2013)
39. R. Aaij et al. [LHCb], Observation of $B_c^+ \rightarrow J/\psi D_s^+$ and $B_c^+ \rightarrow J/\psi D_s^{*+}$ decays. *Phys. Rev. D* **87**, 112012 (2013)
40. R. Aaij et al. [LHCb], First observation of the decay $B_c^+ \rightarrow J/\psi K^+$. *JHEP* **09**, 075 (2013)
41. R. Aaij et al. [LHCb], Observation of the decay $B_c^+ \rightarrow B_s^0 \pi^+$. *Phys. Rev. Lett.* **111**, 181801 (2013)
42. R. Aaij et al. [LHCb], Observation of the decay $B_c \rightarrow J/\psi K^+ K^- \pi^+$. *JHEP* **11**, 094 (2013)
43. G. Aad et al. [ATLAS], Observation of an excited B_c^\pm meson state with the ATLAS detector. *Phys. Rev. Lett.* **113**, 212004 (2014)
44. A.M. Sirunyan et al. [CMS], Observation of two excited B_c^+ states and measurement of the $B_c^+(2S)$ mass in pp collisions at $\sqrt{s} = 13$ TeV. *Phys. Rev. Lett.* **122**, 132001 (2019)
45. R. Aaij et al. [LHCb], Observation of an excited B_c^+ state. *Phys. Rev. Lett.* **122**, 232001 (2019)
46. R.L. Workman et al. [Particle Data Group], Review of particle physics. *PTEP* **2022**, 083C01 (2022)
47. S. Godfrey, N. Isgur, Mesons in a relativized quark model with chromodynamics. *Phys. Rev. D* **32**, 189–231 (1985)
48. E.J. Eichten, C. Quigg, Mesons with beauty and charm: spectroscopy. *Phys. Rev. D* **49**, 5845–5856 (1994)
49. S.S. Gershtein, V.V. Kiselev, A.K. Likhoded, A.V. Tkabladze, B_c spectroscopy. *Phys. Rev. D* **51**, 3613–3627 (1995)
50. L.P. Fulcher, Phenomenological predictions of the properties of the B_c system. *Phys. Rev. D* **60**, 074006 (1999)
51. D. Ebert, R.N. Faustov, V.O. Galkin, Properties of heavy quarkonia and B_c mesons in the relativistic quark model. *Phys. Rev. D* **67**, 014027 (2003)
52. S. Godfrey, Spectroscopy of B_c mesons in the relativized quark model. *Phys. Rev. D* **70**, 054017 (2004)
53. E.J. Eichten, C. Quigg, Mesons with beauty and charm: new horizons in spectroscopy. *Phys. Rev. D* **99**(5), 054025 (2019)
54. E. van Beveren, G. Rupp, Observed $D_s(2317)$ and tentative $D(2100-2300)$ as the charmed cousins of the light scalar nonet. *Phys. Rev. Lett.* **91**, 012003 (2003)

55. Y.B. Dai, C.S. Huang, C. Liu, S.L. Zhu, Understanding the D_{sJ}^+ (2317) and D_{sJ}^+ (2460) with sum rules in HQET. *Phys. Rev. D* **68**, 114011 (2003)
56. D.S. Hwang, D.W. Kim, Mass of D_{sJ}^* (2317) and coupled channel effect. *Phys. Lett. B* **601**, 137–143 (2004)
57. Y.A. Simonov, J.A. Tjon, The coupled-channel analysis of the D and D_s mesons. *Phys. Rev. D* **70**, 114013 (2004)
58. P.G. Ortega, J. Segovia, D.R. Entem, F. Fernandez, Molecular components in P -wave charmed-strange mesons. *Phys. Rev. D* **94**(7), 074037 (2016)
59. I.V. Danilkin, Y.A. Simonov, Dynamical origin and the pole structure of X (3872). *Phys. Rev. Lett.* **105**, 102002 (2010)
60. B.Q. Li, C. Meng, K.T. Chao, Coupled-channel and screening effects in charmonium spectrum. *Phys. Rev. D* **80**, 014012 (2009)
61. Y.S. Kalashnikova, Coupled-channel model for charmonium levels and an option for X (3872). *Phys. Rev. D* **72**, 034010 (2005)
62. S.Q. Luo, B. Chen, Z.W. Liu, X. Liu, Resolving the low mass puzzle of $\Lambda_c(2940)^+$. *Eur. Phys. J. C* **80**, 301 (2020)
63. Q.T. Song, D.Y. Chen, X. Liu, T. Matsuki, Charmed-strange mesons revisited: mass spectra and strong decays. *Phys. Rev. D* **91**, 054031 (2015)
64. Q.T. Song, D.Y. Chen, X. Liu, T. Matsuki, Higher radial and orbital excitations in the charmed meson family. *Phys. Rev. D* **92**, 074011 (2015)
65. J.Z. Wang, Z.F. Sun, X. Liu, T. Matsuki, Higher bottomonium zoo. *Eur. Phys. J. C* **78**, 915 (2018)
66. J.Z. Wang, D.Y. Chen, X. Liu, T. Matsuki, Constructing J/ψ family with updated data of charmoniumlike Y states. *Phys. Rev. D* **99**, 114003 (2019)
67. J.Z. Wang, R.Q. Qian, X. Liu, T. Matsuki, Are the Y states around 4.6 GeV from e^+e^- annihilation higher charmonia? *Phys. Rev. D* **101**, 034001 (2020)
68. K.T. Chao, Y.B. Ding, D.H. Qin, Possible phenomenological indication for the string Coulomb term and the color screening effects in the quark-anti-quark potential. *Commun. Theor. Phys.* **18**, 321–326 (1992)
69. Y.B. Ding, K.T. Chao, D.H. Qin, Screened $Q - \bar{Q}$ potential and spectrum of heavy quarkonium. *Chin. Phys. Lett.* **10**, 460–463 (1993)
70. M.X. Duan, X. Liu, Where are 3P and higher P-wave states in the charmonium family? *Phys. Rev. D* **104**(7), 074010 (2021)
71. M.X. Duan, S.Q. Luo, X. Liu, T. Matsuki, Possibility of charmoniumlike state X (3915) as $\chi_{c0}(2P)$ state. *Phys. Rev. D* **101**, 054029 (2020)
72. L. Micu, Decay rates of meson resonances in a quark model. *Nucl. Phys. B* **10**, 521–526 (1969)
73. A. Le Yaouanc, L. Oliver, O. Pene, J.C. Raynal, Naive quark pair creation model of strong interaction vertices. *Phys. Rev. D* **8**, 2223–2234 (1973)
74. E.S. Ackleh, T. Barnes, E.S. Swanson, On the mechanism of open flavor strong decays. *Phys. Rev. D* **54**, 6811–6829 (1996)
75. H.G. Blundell, Meson properties in the quark model: a look at some outstanding problems. [arXiv:hep-ph/9608473](https://arxiv.org/abs/hep-ph/9608473)
76. C.Q. Pang, J.Z. Wang, X. Liu, T. Matsuki, A systematic study of mass spectra and strong decay of strange mesons. *Eur. Phys. J. C* **77**, 861 (2017)
77. L.M. Wang, S.Q. Luo, X. Liu, Light unflavored vector meson spectroscopy around the mass range of 2.4~3 GeV and possible experimental evidence. *Phys. Rev. D* **105**, 034011 (2022)
78. W. Lucha, F.F. Schoberl, D. Gromes, Bound states of quarks. *Phys. Rep.* **200**, 127–240 (1991)
79. E. Eichten, K. Gottfried, T. Kinoshita, J.B. Kogut, K.D. Lane, T.M. Yan, The spectrum of charmonium. *Phys. Rev. Lett.* **36**, 1276 (1976)
80. R. Ding, B.D. Wan, Z.Q. Chen, G.L. Wang, C.F. Qiao, Finding $B_c(3S)$ states via their strong decays. *Phys. Lett. B* **816**, 136277 (2021)
81. G.L. Wang, T. Wang, Q. Li, C.H. Chang, The mass spectrum and wave functions of the B_c system. *JHEP* **05**, 006 (2022)
82. A. Le Yaouanc, L. Oliver, O. Pene, J.C. Raynal, Naive quark pair creation model and baryon decays. *Phys. Rev. D* **9**, 1415–1419 (1974)
83. A. Le Yaouanc, L. Oliver, O. Pene, J.C. Raynal, Resonant Partial wave amplitudes in $\pi N \rightarrow \pi\pi N$ according to the naive quark pair creation model. *Phys. Rev. D* **11**, 1272 (1975)
84. A. Le Yaouanc, L. Oliver, O. Pene, J.C. Raynal, Strong decays of $\psi''(4.028)$ as a radial excitation of charmonium. *Phys. Lett. B* **71**, 397–399 (1977)
85. M. Jacob, G.C. Wick, On the general theory of collisions for particles with spin. *Ann. Phys.* **7**, 404–428 (1959)
86. C. Hayne, N. Isgur, Beyond the wave function at the origin: some momentum dependent effects in the nonrelativistic quark model. *Phys. Rev. D* **25**, 1944 (1982)
87. Q. Li, M.S. Liu, L.S. Lu, Q.F. Lü, L.C. Gui, X.H. Zhong, Excited bottom-charmed mesons in a nonrelativistic quark model. *Phys. Rev. D* **99**, 096020 (2019)
88. T.M. Yan, Hadronic transitions between heavy quark states in quantum chromodynamics. *Phys. Rev. D* **22**, 1652 (1980)
89. H.Y. Zhou, Y.P. Kuang, Coupled channel effects in hadronic transitions in heavy quarkonium systems. *Phys. Rev. D* **44**, 756–769 (1991)
90. Y.P. Kuang, T.M. Yan, Predictions for hadronic transitions in the $b\bar{b}$ system. *Phys. Rev. D* **24**, 2874 (1981)
91. Y.P. Kuang, QCD multipole expansion and hadronic transitions in heavy quarkonium systems. *Front. Phys. China* **1**, 19–37 (2006)
92. S. Godfrey, K. Moats, Bottomonium mesons and strategies for their observation. *Phys. Rev. D* **92**, 054034 (2015)
93. J. Segovia, P.G. Ortega, D.R. Entem, F. Fernández, Bottomonium spectrum revisited. *Phys. Rev. D* **93**, 074027 (2016)
94. B. Wang, H. Xu, X. Liu, D.Y. Chen, S. Coito, E. Eichten, Using $X(3823) \rightarrow J/\psi\pi^+\pi^-$ to identify coupled-channel effects. *Front. Phys. (Beijing)* **11**, 111402 (2016)
95. R. Giles, S.H.H. Tye, The application of the quark-confining string to the ψ spectroscopy. *Phys. Rev. D* **16**, 1079 (1977)
96. S.H.H. Tye, A quark-binding string. *Phys. Rev. D* **13**, 3416 (1976)
97. W. Buchmüller, S.H.H. Tye, Vibrational states in the Υ spectroscopy. *Phys. Rev. Lett.* **44**, 850–853 (1980)
98. S. Capstick, N. Isgur, Baryons in a relativized quark model with chromodynamics. *AIP Conf. Proc.* **132**, 267–271 (1985)
99. B. Martín-González, P.G. Ortega, D.R. Entem, F. Fernández, J. Segovia, Toward the discovery of novel B_c states: radiative and hadronic transitions. *Phys. Rev. D* **106**, 054009 (2022)
100. H. Mendez et al. [CLEO], Branching fractions for transitions of $\psi(2S)$ to J/ψ . *Phys. Rev. D* **78**, 011102 (2008)
101. N.E. Adam et al. [CLEO], Observation of $\psi(3770) \rightarrow \pi\pi J/\psi$ and measurement of $\Gamma_{ee}[\psi(2S)]$. *Phys. Rev. Lett.* **96**, 082004 (2006)
102. F. Butler et al. [CLEO], Analysis of hadronic transitions in $\Upsilon(3S)$ decays. *Phys. Rev. D* **49**, 40–57 (1994)
103. J.P. Alexander et al. [CLEO], The hadronic transitions $\Upsilon(2S) \rightarrow \Upsilon(1S)$. *Phys. Rev. D* **58**, 052004 (1998)
104. E. Guido et al. [Belle], Study of η and dipion transitions in $\Upsilon(4S)$ decays to lower bottomonia. *Phys. Rev. D* **96**, 052005 (2017)
105. D.Y. Chen, X. Liu, X.Q. Li, Anomalous dipion invariant mass distribution of the $\Upsilon(4S)$ decays into $\Upsilon(1S)\pi^+\pi^-$ and $\Upsilon(2S)\pi^+\pi^-$. *Eur. Phys. J. C* **71**, 1808 (2011)
106. D.Y. Chen, J. He, X.Q. Li, X. Liu, Dipion invariant mass distribution of the anomalous $\Upsilon(1S)\pi^+\pi^-$ and $\Upsilon(2S)\pi^+\pi^-$ production near the peak of $\Upsilon(10860)$. *Phys. Rev. D* **84**, 074006 (2011)

107. Z.Y. Bai, Y.S. Li, Q. Huang, X. Liu, T. Matsuki, $\Upsilon(10753) \rightarrow \Upsilon(nS)\pi^+\pi^-$ decays induced by hadronic loop mechanism. *Phys. Rev. D* **105**, 074007 (2022)
108. P. Moxhay, Coupled channel effects in the decay $\Upsilon(3S) \rightarrow \Upsilon(1S)\pi^+\pi^-$. *Phys. Rev. D* **39**, 3497 (1989)
109. C. Meng, K.T. Chao, Scalar resonance contributions to the dipion transition rates of $\Upsilon(4S, 5S)$ in the re-scattering model. *Phys. Rev. D* **77**, 074003 (2008)
110. C. Meng, K.T. Chao, Peak shifts due to $B^{(*)}-\bar{B}^{(*)}$ rescattering in $\Upsilon(5S)$ dipion transitions. *Phys. Rev. D* **78**, 034022 (2008)
111. D.Y. Chen, X. Liu, S.L. Zhu, Charged bottomonium-like states $Z_b(10610)$ and $Z_b(10650)$ and the $\Upsilon(5S) \rightarrow \Upsilon(2S)\pi^+\pi^-$ decay. *Phys. Rev. D* **84**, 074016 (2011)
112. I.V. Danilkin, V.D. Orlovsky, Y.A. Simonov, Hadron interaction with heavy quarkonia. *Phys. Rev. D* **85**, 034012 (2012)
113. D.Y. Chen, X. Liu, T. Matsuki, Charged bottomonium-like structures in the hidden-bottom dipion decays of $\Upsilon(11020)$. *Phys. Rev. D* **84**, 074032 (2011)
114. D.Y. Chen, X. Liu, T. Matsuki, η transitions between charmonia with meson loop contributions. *Phys. Rev. D* **87**, 054006 (2013)
115. D.Y. Chen, X. Liu, T. Matsuki, Explaining the anomalous $\Upsilon(5S) \rightarrow \chi_{bJ}\omega$ decays through the hadronic loop effect. *Phys. Rev. D* **90**, 034019 (2014)
116. D.Y. Chen, X. Liu, T. Matsuki, Observation of $e^+e^- \rightarrow \chi_{c0}\omega$ and missing higher charmonium $\psi(4S)$. *Phys. Rev. D* **91**, 094023 (2015)
117. B. Wang, X. Liu, D.Y. Chen, Prediction of anomalous $\Upsilon(5S) \rightarrow \Upsilon(1^3D_J)\eta$ transitions. *Phys. Rev. D* **94**, 094039 (2016)
118. Q. Huang, B. Wang, X. Liu, D.Y. Chen, T. Matsuki, Exploring the $\Upsilon(6S) \rightarrow \chi_{bJ}\phi$ and $\Upsilon(6S) \rightarrow \chi_{bJ}\omega$ hidden-bottom hadronic transitions. *Eur. Phys. J. C* **77**, 165 (2017)
119. Q. Huang, H. Xu, X. Liu, T. Matsuki, Potential observation of the $\Upsilon(6S) \rightarrow \Upsilon(1^3D_J)\eta$ transitions at Belle II. *Phys. Rev. D* **97**, 094018 (2018)
120. Q. Huang, X. Liu, T. Matsuki, Proposal of searching for the $\Upsilon(6S)$ hadronic decays into $\Upsilon(nS)$ plus $\eta^{(\prime)}$. *Phys. Rev. D* **98**, 054008 (2018)
121. Y.S. Li, Z.Y. Bai, Q. Huang, X. Liu, Hidden-bottom hadronic decays of $\Upsilon(10753)$ with a $\eta^{(\prime)}$ or ω emission. *Phys. Rev. D* **104**, 034036 (2021)
122. Y.S. Li, Z.Y. Bai, X. Liu, Investigating the $\Upsilon(10753) \rightarrow \Upsilon(1^3D_J)\eta$ transitions. *Phys. Rev. D* **105**, 114041 (2022)
123. S.J. Brodsky, J.R. Primack, The electromagnetic interactions of composite systems. *Ann. Phys.* **52**, 315–365 (1969)
124. W. Kwong, J.L. Rosner, D wave quarkonium levels of the Υ family. *Phys. Rev. D* **38**, 279 (1988)
125. V.A. Novikov, L.B. Okun, M.A. Shifman, A.I. Vainshtein, M.B. Voloshin, V.I. Zakharov, Charmonium and gluons: basic experimental facts and theoretical introduction. *Phys. Rep.* **41**, 1–133 (1978)
126. F. Schlumpf, Magnetic moments of the baryon decuplet in a relativistic quark model. *Phys. Rev. D* **48**, 4478–4480 (1993)
127. S. Kumar, R. Dhir, R.C. Verma, Magnetic moments of charm baryons using effective mass and screened charge of quarks. *J. Phys. G* **31**, 141–147 (2005)
128. G. Ramalho, K. Tsushima, F. Gross, A Relativistic quark model for the Omega-electromagnetic form factors. *Phys. Rev. D* **80**, 033004 (2009)
129. M.W. Li, Z.W. Liu, Z.F. Sun, R. Chen, Magnetic moments and transition magnetic moments of P_c and P_{cs} states. *Phys. Rev. D* **104**, 054016 (2021)
130. F.L. Wang, H.Y. Zhou, Z.W. Liu, X. Liu, What can we learn from the electromagnetic properties of hidden-charm molecular pentaquarks with single strangeness? *Phys. Rev. D* **106**, 054020 (2022)
131. F.L. Wang, H.Y. Zhou, Z.W. Liu, X. Liu, Exploring the electromagnetic properties of the $\Xi_c^{(\prime,*)}\bar{D}_s^*$ and $\Omega_c^{(*)}\bar{D}_s^*$ molecular states. *Phys. Rev. D* **108**, 034006 (2023)
132. C. Deng, S.L. Zhu, T_{cc}^+ and its partners. *Phys. Rev. D* **105**, 054015 (2022)
133. F. Gao, H.S. Li, Magnetic moments of the hidden-charm strange pentaquark states. *Chin. Phys. C* **46**, 123111 (2022)
134. S.L. Zhu, Pentaquarks. *Int. J. Mod. Phys. A* **19**, 3439–3469 (2004)
135. A.R. Haghpayma, Magnetic moment of the pentaquark Θ^+ state. [arXiv:hep-ph/0609253](https://arxiv.org/abs/hep-ph/0609253)
136. F. Schlumpf, Relativistic constituent quark model of electroweak properties of baryons. *Phys. Rev. D* **47**, 4114 (1993). Erratum: *Phys. Rev. D* **49**, 6246 (1994)
137. T.P. Cheng, L.F. Li, Why naive quark model can yield a good account of the baryon magnetic moments. *Phys. Rev. Lett.* **80**, 2789–2792 (1998)
138. P. Ha, L. Durand, Baryon magnetic moments in a QCD based quark model with loop corrections. *Phys. Rev. D* **58**, 093008 (1998)
139. R. Dhir, R.C. Verma, Magnetic moments of ($J^P = 3/2^+$) heavy baryons using effective mass scheme. *Eur. Phys. J. A* **42**, 243–249 (2009)
140. A. Majethiya, B. Patel, P.C. Vinodkumar, Radiative decays of single heavy flavour baryons. *Eur. Phys. J. A* **42**, 213–218 (2009)
141. N. Sharma, H. Dahiya, P.K. Chatley, M. Gupta, Spin $\frac{1}{2}^+$, spin $\frac{3}{2}^+$ and transition magnetic moments of low lying and charmed baryons. *Phys. Rev. D* **81**, 073001 (2010)
142. N. Sharma, A. Martinez Torres, K.P. Khemchandani, H. Dahiya, Magnetic moments of the low-lying $1/2^-$ octet baryon resonances. *Eur. Phys. J. A* **49**, 11 (2013)
143. R. Dhir, C.S. Kim, R.C. Verma, Magnetic moments of bottom baryons: effective mass and screened charge. *Phys. Rev. D* **88**, 094002 (2013)
144. Z. Ghaleynovi, A.A. Rajabi, S.X. Qin, D.H. Rischke, Ground-state masses and magnetic moments of heavy baryons. *Mod. Phys. Lett. A* **29**, 1450106 (2014)
145. A. Girdhar, H. Dahiya, M. Randhawa, Magnetic moments of $J^P = \frac{3}{2}^+$ decuplet baryons using effective quark masses in chiral constituent quark model. *Phys. Rev. D* **92**, 033012 (2015)
146. A. Majethiya, K. Thakkar, P.C. Vinodkumar, Spectroscopy and decay properties of Σ_b , Λ_b baryons in quark-diquark model. *Chin. J. Phys.* **54**, 495–502 (2016)
147. K. Thakkar, A. Majethiya, P.C. Vinodkumar, Magnetic moments of baryons containing all heavy quarks in the quark-diquark model. *Eur. Phys. J. Plus* **131**, 339 (2016)
148. Z. Shah, K. Thakkar, A.K. Rai, P.C. Vinodkumar, Mass spectra and Regge trajectories of Λ_c^+ , Σ_c^0 , Ξ_c^0 and Ω_c^0 baryons. *Chin. Phys. C* **40**, 123102 (2016)
149. Z. Shah, K. Thakkar, A.K. Rai, Excited state mass spectra of doubly heavy baryons Ω_{cc} , Ω_{bb} and Ω_{bc} . *Eur. Phys. J. C* **76**, 530 (2016)
150. A. Kaur, P. Gupta, A. Upadhyay, Properties of $J^P = 1/2^+$ baryon octets at low energy. *PTEP* **2017**, 063B02 (2017)
151. Z. Shah, A. Kumar Rai, Spectroscopy of the Ω_{ccb} baryon in the hypercentral constituent quark model. *Chin. Phys. C* **42**, 053101 (2018)
152. K. Gandhi, Z. Shah, A.K. Rai, Decay properties of singly charmed baryons. *Eur. Phys. J. Plus* **133**, 512 (2018)
153. H. Dahiya, Transition magnetic moments of $J^P = \frac{3}{2}^+$ decuplet to $J^P = \frac{1}{2}^+$ octet baryons in the chiral constituent quark model. *Chin. Phys. C* **42**, 093102 (2018)
154. V. Šimonis, Improved predictions for magnetic moments and M1 decay widths of heavy hadrons. [arXiv:1803.01809](https://arxiv.org/abs/1803.01809)

155. Z. Ghalenovi, M. Moazzen Sorkhi, Mass spectra and decay properties of Σ_b and Λ_b baryons in a quark model. *Eur. Phys. J. Plus* **133**, 301 (2018)
156. K. Gandhi, A.K. Rai, Spectrum of strange singly charmed baryons in the constituent quark model. *Eur. Phys. J. Plus* **135**, 213 (2020)
157. S. Rahmani, H. Hassanabadi, H. Sobhani, Mass and decay properties of double heavy baryons with a phenomenological potential model. *Eur. Phys. J. C* **80**, 312 (2020)
158. A. Hazra, S. Rakshit, R. Dhir, Radiative M1 transitions of heavy baryons: effective quark mass scheme. *Phys. Rev. D* **104**, 053002 (2021)
159. C. Menapara, A.K. Rai, Spectroscopic investigation of light strange $S = -1$ Λ , Σ and $S = -2$ Ξ baryons. *Chin. Phys. C* **45**, 063108 (2021)
160. C. Menapara, A.K. Rai, Spectroscopic study of Strangeness = -3 Ω^- baryon. *Chin. Phys. C* **46**, 103102 (2022)
161. H. Mutuk, The status of Ξ_{cc}^{++} baryon: investigating quark-diquark model. *Eur. Phys. J. Plus* **137**, 10 (2022)
162. C. Menapara, A.K. Rai, Spectroscopy of light baryons: Δ resonances. *Int. J. Mod. Phys. A* **37**, 2250177 (2022)
163. B. Mohan, T.M.S., A. Hazra, R. Dhir, Screening of the quark charge and mixing effects on transition moments and M1 decay widths of baryons. *Phys. Rev. D* **106**, 113007 (2022)
164. H.T. An, S.Q. Luo, Z.W. Liu, X. Liu, Spectroscopy behavior of fully heavy tetraquarks. [arXiv:2208.03899](https://arxiv.org/abs/2208.03899)
165. T.W. Wu, Y.L. Ma, Doubly heavy tetraquark multiplets as heavy antiquark-diquark symmetry partners of heavy baryons. [arXiv:2211.15094](https://arxiv.org/abs/2211.15094)
166. A. Kakadiya, Z. Shah, A.K. Rai, Spectroscopy of Ω_{ccc} and Ω_{bbb} baryons. *Int. J. Mod. Phys. A* **37**, 2250225 (2022)
167. F.L. Wang, S.Q. Luo, X. Liu, Radiative decays and magnetic moments of the predicted B_c -like molecules. *Phys. Rev. D* **107**(11), 114017 (2023)
168. H.Y. Zhou, F.L. Wang, Z.W. Liu, X. Liu, Probing the electromagnetic properties of the $\Sigma_c^{(*)} D^{(*)}$ -type doubly charmed molecular pentaquarks. *Phys. Rev. D* **106**, 034034 (2022)
169. G.J. Wang, R. Chen, L. Ma, X. Liu, S.L. Zhu, Magnetic moments of the hidden-charm pentaquark states. *Phys. Rev. D* **94**, 094018 (2016)
170. Y.R. Liu, P.Z. Huang, W.Z. Deng, X.L. Chen, S.L. Zhu, Pentaquark magnetic moments in different models. *Phys. Rev. C* **69**, 035205 (2004)
171. P.Z. Huang, Y.R. Liu, W.Z. Deng, X.L. Chen, S.L. Zhu, Heavy pentaquarks. *Phys. Rev. D* **70**, 034003 (2004)
172. D.B. Lichtenberg, Magnetic moments of charmed baryons in the quark model. *Phys. Rev. D* **15**, 345 (1977)
173. H.S. Li, L. Meng, Z.W. Liu, S.L. Zhu, Magnetic moments of the doubly charmed and bottom baryons. *Phys. Rev. D* **96**, 076011 (2017)
174. L. Meng, H.S. Li, Z.W. Liu, S.L. Zhu, Magnetic moments of the spin- $\frac{3}{2}$ doubly heavy baryons. *Eur. Phys. J. C* **77**, 869 (2017)
175. H.S. Li, L. Meng, Z.W. Liu, S.L. Zhu, Radiative decays of the doubly charmed baryons in chiral perturbation theory. *Phys. Lett. B* **777**, 169–176 (2018)
176. B. Wang, B. Yang, L. Meng, S.L. Zhu, Radiative transitions and magnetic moments of the charmed and bottom vector mesons in chiral perturbation theory. *Phys. Rev. D* **100**, 016019 (2019)
177. V. Šimonis, Magnetic properties of ground-state mesons. *Eur. Phys. J. A* **52**, 90 (2016)
178. Z.F. Sun, X. Liu, M. Nielsen, S.L. Zhu, Hadronic molecules with both open charm and bottom. *Phys. Rev. D* **85**, 094008 (2012)
179. A. Lytle, B. Colquhoun, C. Davies, J. Koponen, C. McNeile, Semileptonic B_c decays from full lattice QCD. *PoS BEAUTY2016*, 069 (2016)
180. J. Harrison et al. [HPQCD], $B_c \rightarrow J/\psi$ form factors for the full q^2 range from lattice QCD. *Phys. Rev. D* **102**, 094518 (2020)
181. X.Q. Hu, S.P. Jin, Z.J. Xiao, Semileptonic decays $B_c \rightarrow (\eta_c, J/\psi)l\bar{\nu}_l$ in the “PQCD + Lattice” approach. *Chin. Phys. C* **44**, 023104 (2020)
182. X. Liu, The B_c -meson decays into J/ψ plus a light meson in the iPQCD formalism. [arXiv:2305.00713](https://arxiv.org/abs/2305.00713)
183. D. Leljak, B. Melic, M. Patra, On lepton flavour universality in semileptonic $B_c \rightarrow \eta_c, J/\psi$ decays. *JHEP* **05**, 094 (2019)
184. V.V. Kiselev, Exclusive decays and lifetime of B_c meson in QCD sum rules. [arXiv:hep-ph/0211021](https://arxiv.org/abs/hep-ph/0211021)
185. T. Huang, F. Zuo, Semileptonic B_c decays and charmonium distribution amplitude. *Eur. Phys. J. C* **51**, 833–839 (2007)
186. D. Scora, N. Isgur, Semileptonic meson decays in the quark model: an update. *Phys. Rev. D* **52**, 2783–2812 (1995)
187. P. Colangelo, F. De Fazio, Using heavy quark spin symmetry in semileptonic B_c decays. *Phys. Rev. D* **61**, 034012 (2000)
188. M.A. Ivanov, J.G. Korner, P. Santorelli, The semileptonic decays of the B_c meson. *Phys. Rev. D* **63**, 074010 (2001)
189. D. Ebert, R.N. Faustov, V.O. Galkin, Weak decays of the B_c meson to charmonium and D mesons in the relativistic quark model. *Phys. Rev. D* **68**, 094020 (2003)
190. M.A. Ivanov, J.G. Korner, P. Santorelli, Exclusive semileptonic and nonleptonic decays of the B_c meson. *Phys. Rev. D* **73**, 054024 (2006)
191. W. Wang, Y.L. Shen, C.D. Lu, The study of $B_c^- \rightarrow X(3872)\pi^- (K^-)$ decays in the covariant light-front approach. *Eur. Phys. J. C* **51**, 841–847 (2007)
192. W. Wang, Y.L. Shen, C.D. Lu, Covariant light-front approach for B_c transition form factors. *Phys. Rev. D* **79**, 054012 (2009)
193. X.X. Wang, W. Wang, C.D. Lu, B_c to p -wave charmonia transitions in covariant light-front approach. *Phys. Rev. D* **79**, 114018 (2009)
194. H.W. Ke, T. Liu, X.Q. Li, Transitions of $B_c \rightarrow \psi(1S, 2S)$ and the modified harmonic oscillator wave function in LFM. *Phys. Rev. D* **89**, 017501 (2014)
195. Y.J. Shi, W. Wang, Z.X. Zhao, $B_c \rightarrow B_{sJ}$ form factors and B_c decays into B_{sJ} in covariant light-front approach. *Eur. Phys. J. C* **76**, 555 (2016)
196. L. Chen, Y.W. Ren, L.T. Wang, Q. Chang, Form factors of $P \rightarrow T$ transition within the light-front quark models. *Eur. Phys. J. C* **82**, 451 (2022)
197. Z.Q. Zhang, Z.J. Sun, Y.C. Zhao, Y.Y. Yang, Z.Y. Zhang, Covariant light-front approach for B_c decays into charmonium: Implications on form factors and branching ratios. [arXiv:2301.11107](https://arxiv.org/abs/2301.11107)
198. Z.J. Sun, S.Y. Wang, Z.Q. Zhang, Y.Y. Yang, Z.Y. Zhang, Semileptonic B_c meson decays to S-wave charmonia and $X(3872)$ within the covariant light-front approach. [arXiv:2308.03114](https://arxiv.org/abs/2308.03114)
199. Z.Q. Yao, D. Binosi, Z.F. Cui, C.D. Roberts, Semileptonic $B_c \rightarrow \eta_c J/\psi$ transitions. *Phys. Lett. B* **818**, 136344 (2021)
200. M. Wirbel, B. Stech, M. Bauer, Exclusive semileptonic decays of heavy mesons. *Z. Phys. C* **29**, 637 (1985)
201. W. Jaus, Covariant analysis of the light front quark model. *Phys. Rev. D* **60**, 054026 (1999)
202. H.Y. Cheng, C.K. Chua, C.W. Hwang, Covariant light front approach for s -wave and p -wave mesons: its application to decay constants and form-factors. *Phys. Rev. D* **69**, 074025 (2004)
203. R.C. Verma, Decay constants and form factors of s -wave and p -wave mesons in the covariant light-front quark model. *J. Phys. G* **39**, 025005 (2012)
204. C. Bourrely, I. Caprini, L. Lellouch, Model-independent description of $B \rightarrow \pi \ell \nu$ decays and a determination of $|V_{ub}|$. *Phys. Rev. D* **82**, 099902 (2010)
205. K. Chen, H.W. Ke, X. Liu, T. Matsuki, Estimating the production rates of D -wave charmed mesons via the semileptonic decays of bottom mesons. *Chin. Phys. C* **43**, 023106 (2019)

206. A. Khodjamirian, T. Mannel, A.A. Pivovarov, Y.M. Wang, Charm-loop effect in $B \rightarrow K^{(*)} \ell^+ \ell^-$ and $B \rightarrow K^* \gamma$. JHEP **09**, 089 (2010)
207. S. Cheng, A. Khodjamirian, J. Virto, $B \rightarrow \pi\pi$ form factors from light-cone sum rules with B -meson distribution amplitudes. JHEP **05**, 157 (2017)
208. R. Aaij et al. [LHCb], Measurement of the ratio of branching ratios $\mathcal{B}(B_c^+ \rightarrow J/\psi \tau^+ \nu_\tau)/\mathcal{B}(B_c^+ \rightarrow J/\psi \mu^+ \nu_\mu)$. Phys. Rev. Lett. **120**, 121801 (2018)
209. R. Aaij et al. [LHCb], Study of B_c^+ decays to the $K^+ K^- \pi^+$ final state and evidence for the decay $B_c^+ \rightarrow \chi_{c0} \pi^+$. Phys. Rev. D **94**, 091102 (2016)
210. E.H. Mezoir, P. Gonzalez, Is the spectrum of highly excited mesons purely coulombian? Phys. Rev. Lett. **101**, 232001 (2008)
211. S.Q. Luo, B. Chen, X. Liu, T. Matsuki, Predicting a new resonance as charmed-strange baryonic analog of D_{s0}^* (2317). Phys. Rev. D **103**, 074027 (2021)